Project Number: MQP-SDO-201

Ciliary and Flagellar Dynamics

A Major Qualifying Project Report

Submitted to The Faculty

of

Worcester Polytechnic Institute

In partial fulfillment of the requirements for the

Degree of Bachelor of Science

by

Dana Gowing

April 22, 2013

Approved:

Professor Sarah Olson

Abstract

A study of the factors that regulate ciliary beating was conducted in an effort to better understand the dynamics of cilia and flagella. A model proposed by Charles Lindemann called the Geometric Clutch Hypothesis (GCH) was first analyzed and then extended to incorporate various effects. The model used transverse forces as the primary regulator of dynein attachment as well as a constant force for the force exerted by dynein. After analyzing the original GCH, the model was then extended to incorporate the effects of a time-dependent varying dynein force as well as the effects of calcium (Ca^{2+}). After proposing and implementing two ordinary differential equations (one for a varying dynein force, one for a varying dynein force with the addition of Ca^{2+}), the results were analyzed and are presented in this report. Notable findings included simulations that produced life-like ciliary beating and simulations that were consistent with experimental data regarding the effects of Ca^{2+}.

Executive Summary

Cilia and flagella are cell organelles that serve a critical function in cellular motility. Ciliary beating is characterized by a sweeping-like motion with distinct effective and recovery strokes. The cylindrical axoneme of these cellular appendages houses microtubules and elastic linkers called nexins distributed along the cylinder. Motor proteins acting along the microtubules enable the axoneme to bend. Repeated bending of the axoneme gives rise to the self-propagating "ciliary beat". Dynein is one such motor protein that helps facilitate the coordinated beating of cilia and flagella. Dynein converts ATP into mechanical movement and "walks" along an adjacent microtubule doublet, displacing the doublets. Dynein is an active force generator that is able to bend the cilium due in part to the structural constraints of the axoneme. As dyneins attach to the neighboring microtubule, they "pull" and draw the microtubules closer together. Questions remain about what factors regulate the activation of dyneins.

The goal of this project is to further identify what regulates ciliary and flagellar beating. Furthermore, in an effort to better understand the effects of certain variables on ciliary beating, simulations were generated and compared to experimental data. The model used in these simulations is founded upon the model of ciliary and flagellar beating proposed by Charles Lindemann in 1994. Titled the Geometric Clutch Hypothesis (GCH), the model uses forces as the primary regulator of dynein attachment. When the axoneme bends, forces develop due to structural restraints as well as dynein. The main idea behind the GCH is that when the sum of forces acting along the axoneme reaches a critical value, dynein will either attach or detach. Dynein attaches when doublets are pulled sufficiently close together, and detaches when doublets are pulled sufficiently far apart. In an updated version of the GCH, probabilities of dynein attachment are calculated based upon the force exerted by dynein as well as information from previous segments, incorporating a "zipper" effect.

When analyzing the original GCH model, several modeling parameters were studied. These included parameters with no known experimental value. After changing these values, the resulting beatforms along with other critical variables were compared to the results for the original parameter values. One of the more telling variables analyzed was curvature, which is a measure of how sharply bent the cilium is. For example, when the resting probabilities of dynein attachment are set to different values for the principal and reverse bends, the cilium beats asymmetrically, and the curvature plots show a clear propagation of a wave travelling down the axoneme. When these probabilities are set to the same value, the cilium beats symmetrically about the y-axis, but the clear propagation of a "wave" in the curvature plots is lost.

It has been previously shown and supported by experimental data that the force exerted by dynein can vary greatly. In the original GCH model, forces are calculated based on the number of attached dyneins and the structural properties of the current position of the cilium. Using previous experimental models as a foundation, an ordinary differential equation for a time dependent dynein force was proposed and calculated using sliding velocity. Though four variations of this equation were analyzed, the one that gave the most interesting results involved a cubic term, which is the difference between the current sliding velocity and an average minimum sliding velocity. The waveforms exhibit an increase in symmetry as well as an increase in the range of motion of the cilium. Curvature plots show an overall increase in magnitude, meaning the cilium is more bent. In addition, this differential equation produced radically different beatforms than that of the original GCH even though the change in dynein force from the original GCH model is small. Next, the effects of calcium were studied. Experiments show that calcium changes the waveform, making it more asymmetric. We modified the differential equation to account for a calcium dependent term acting to change the rate of change of

dynein force being generated on a segment. The inclusion of the calcium term was also analyzed and compared to experimental data.

Acknowledgements

I would like to first and foremost thank my project advisor, Professor Sarah Olson, for her unwavering encouragment, support, and guidance. I would also like to thank Dr. Charles Lindemann for his previous work on the subject, which provided an initial model and a deeper understanding of ciliary beating. Finally, I would like to thank the mathematical sciences faculty at WPI for providing me with the necessary mathematical skills and resources to complete this project. I am deeply grateful to have been given this opportunity and look forward to continuing research in the applied mathematical and biological fields.

Contents

List of Figures

List of Tables

Chapter 1

Introduction

Cilia and flagella are cell organelles found primarily in eukaryotic cells (cells that contain a nucleus). A critical function of these appendages is cell motility[16]. For example, the flagellum is the "tail" on sperm that propels the sperm and allows it to swim (figure 1.1 (A))[7]. Cilia are essential not only for cell motility, but also for their sweeping-like motion that is vital for certain organ functions. In humans, for instance, cilia line the trachea, where they assist in clearing mucus out of the lungs (figure 1.1 (B))[20]. The beating of cilia in the fallopian tubes of female mammals is also critical, where the cilia coordinate the movement of an ovum from the ovary to the uterus[19].

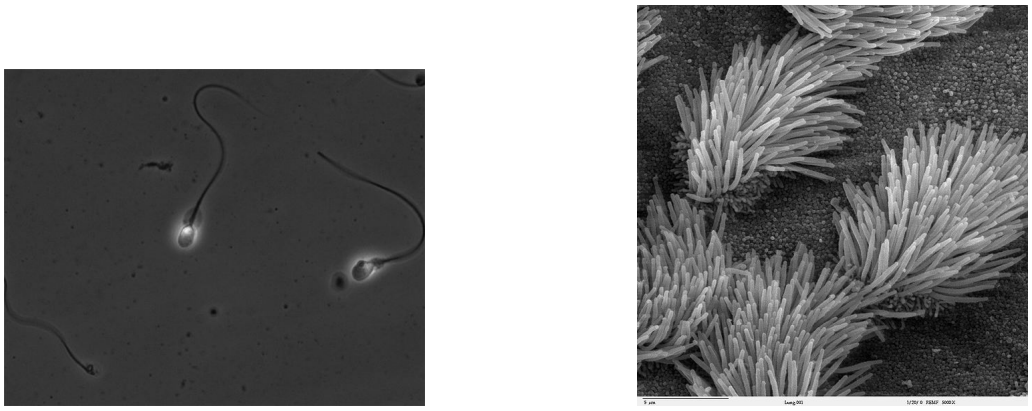

(A) **(B)**

Figure 1.1: (A) Human sperm cells swim in a viscous fluid. The flagella are anchored to the teardrop-shaped cell body of the sperm and bend in varying directions to produce unique waveforms[17]. (B) Ciliated epithelial cells line the trachea. The groups of cilia act as a "broom" to help move fluid and mucus out of the airway and lungs[5].

Cilia and flagella are composed in a "9+2" arrangement in the cylindrical axoneme. The axoneme serves as the skeleton of cilia and flagella, providing both structure and support. Microtubules are a key component of the axoneme: they have a long cylindrical structure and are composed of polymers of tubulin. Within the axoneme, a central pair of microtubules is surrounded by 9 doublet microtubules (figure 1.2 (A))[3]. These doublets are composed of an A tubule and a B tubule which work in conjunction with the other doublets. Motor proteins act along microtubules, allowing the axoneme to bend. Connecting these doublets in a ring around the central pair are highly elastic nexin links.

Furthermore, dyneins are motor proteins that also work as the facilitator of coordinated movement and bending of the doublets and axoneme. Dynein arms extend from the A tubule of one doublet

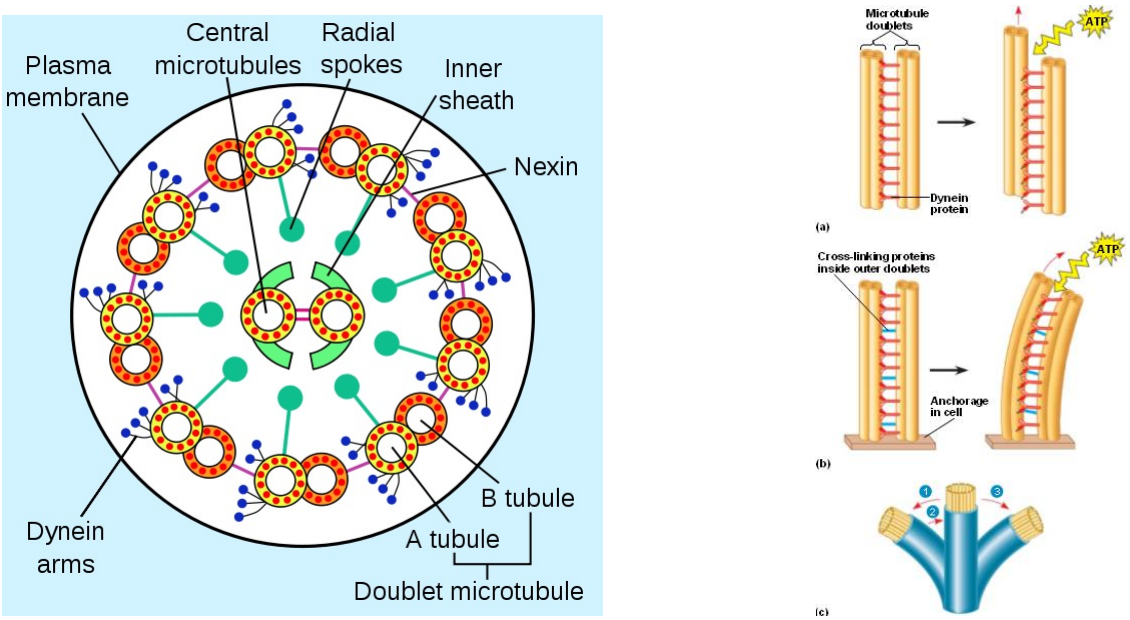

(A) **(B)**

Figure 1.2: (A) A cross-section of an axoneme gives more detail about how microtubule doublets are arranged. Doublets on one side of the axoneme work as a group to bend the axoneme in one direction, while doublets on the opposing side work together to bend it in the opposite direction[15]. (B) Using energy from ATP and converting it into kinetic movement, dyneins "walk" along adjacent microtubules to bend the axoneme[19].

to the B tubule of an adjacent doublet, and, when attached, allow doublets to slide relative to each other[12]. The dyneins accomplish this by converting chemical energy from ATP into kinetic movement and"walk" along the adjacent doublet. Structural restraints of the axoneme, however, prevent doublets from sliding completely apart and result in bending of the axoneme (figure 1.2 (B)). Nexin links and radial spokes are two such restraints, as well as the anchoring of the axoneme to the basal body.

This repeated bending of the axoneme results in what is known as a beat cycle. In cilia, a beat cycle can be best described as a whip-like motion, while in flagella, a beat cycle produces oscillatory waves. To generate a "beat" or oscillation, dyneins must "switch" so doublets can bend in the opposite direction[14]. The microtubules must also work together to coordinate a beat. For example, if one considers the doublets being labeled 1-9 (consecutively), then doublets 1-4 would have dyneins "on" to bend the axoneme one way while the dyneins on doublets 5-9 would be "off", and vice versa. The question that now arises is what regulates the "switching" activity of dyneins to produce coordinated movement. While several hypotheses have been suggested, perhaps the most intriguing and definitive of these is the Geometric Clutch Hypothesis[13].

1.1 The Geometric Clutch Hypothesis

Formulated by Charles Lindemann [13], the Geometric Clutch Hypothesis (GCH) proposes that transverse force acting the length of the axoneme is the primary regulator controlling the active engagement and disengagement of dynein bridges to produce a beat. In summary, transverse forces develop from the bending of the axoneme (figure 1.3). When these forces reach critical values, doublets move sufficiently close to allow dynein attachment and sufficiently far apart to detach dynein bridges. An incorporated "zipper effect" also drives this self-propogating movement: engaged/attached dynein bridges drive neighboring bridges to engage and vice versa. The effect continues until it reaches a point where the transverse force is below a certain cutoff value.

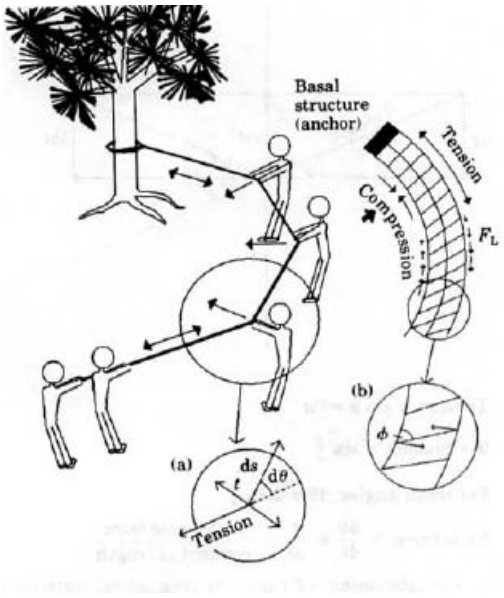

Figure 1.3: Transverse forces develop along the length of an axoneme. As tension increases on one side of the bent axoneme, forces of compression are increasing on the opposite side. The forces felt by the more distal segments (respresented by the two people pulling at the end furthest from the tree) are greater than those felt at basal segments since force accumulates along the length of the axoneme.[13]

In an updated version of the Geometric Clutch Hypothesis, probabilities of dynein bridge attachment are calculated using the force of dyneins as well as information from the previous segment, to incorporate a zipper effect[13]. A third version of the GCH bases the force that the dyneins can produce on the microtubule sliding velocity, with distinctly defined relationships for each of the outer and inner dynein arms. These relationships include Gaussian curves as well as linear functions.

1.2 The Effects of Calcium

The effects of calcium on flagellar and ciliary beating have been widely studied using a variety of methods. While observation and experiments concur that calcium induces asymmetrical beating, the mechanism by which calcium acts is still largely unknown. It has been observed that increases in calcium (Ca^{2+}) induce reversal of swimming direction of sperm by changing the direction of the effective/principal stroke. The increase in asymmetry and quiescence are eventually induced by the inhibition of reverse-bend formation at higher Ca^{2+} concentrations[21]. For example, the beatforms generated by wild-type (normal, no mutations) sperm are typically symmetrical with a constant

amplitude. At higher concentrations of Ca^{2+}, the amplitude of the waveform varies, corresponding to an asymmetrical beatform. For cilia, asymmetry is characterized by the direction in which the cilium beats: if one imagines a cilium staring from a straight, vertical position (i.e, the y-axis on a 2-dimensional graph), then the ratio of how often the cilium beats to the left ($x < 0$) or the right ($x > 0$) would indicate asymmetry.

Three notable calcium pathways affecting ciliary beat frequency have been suggested: Ca^{2+} interacts with calmodulin or *kinases*, blocking calmodulin or phosphatases which changes the CBF; Ca^{2+} interacts with calmodulin or *phosphatases*, blocking calmodulin or phosphatases which changes the CBF; and Ca^{2+} stimulating a ciliary response element which thereby changes the CBF[18]. Previously identified classes of Ca^{2+}-binding proteins include calmodulin (CaM) located in the radial spokes, centrin and caltractin located on the inner dynein arms, and ODA-DC3 and an 18-kDa light chain (LC4) both located on the outer dynein arms as shown in figure 1.4. Calmodulin-binding proteins are located in the central apparatus, the radial spokes, and at the base of the radial spokes[6].

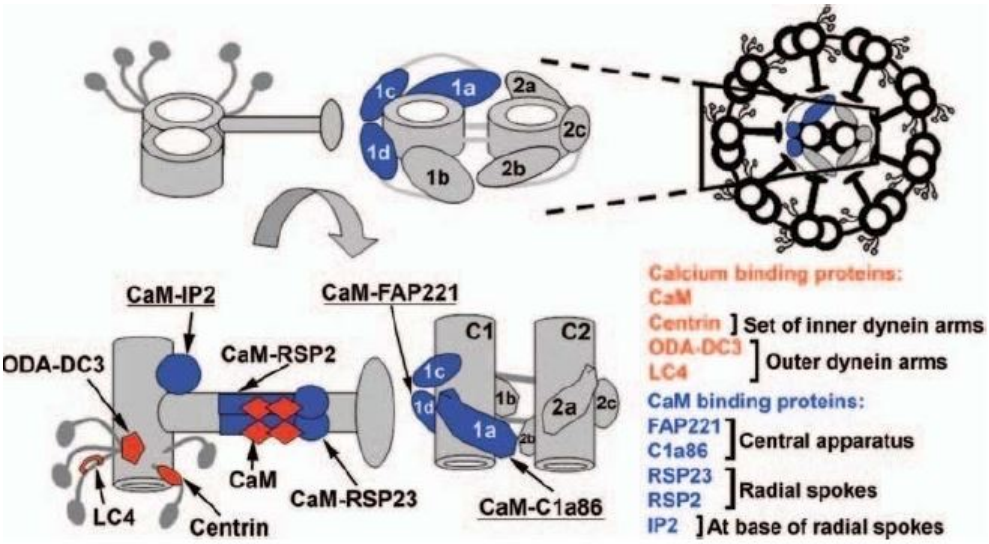

Figure 1.4: Known calcium-binding proteins: the central apparatus and a single microtubule doublet with dynein arms are shown in the top left figure, then rotated and enlarged to show the sites of calcium and calmodulin-binding protein. The bottom left figure shows these proteins located on the microtubule, radial spoke, and dynein arms. The bottom right figure shows the location of these proteins on the central apparatus/pair. [6]

The effects of calcium on microtubule sliding velocity in cilia are less studied. The general decrease in sliding velocity upon the addition of calcium can perhaps be explained by the significant decrease in the angle of the reverse bend and the unchanged angle of the principal bend. Calcium also decreased the maximum sliding velocity more significantly in the middle region of the flagella[1]. Interestingly enough, in low calcium concentrations, dynein activity was reduced in mutants lacking the entire central apparatus . However, in high calcium concentrations, dynein activity was restored to wild-type levels in the same mutants[23].

One of the goals of this research is to study the effects of Ca^{2+} on cilia more in depth. Using a simulation of a cilium coded in Matlab based on the Geometric Clutch Hypothesis as a starting point, working with different parameters and relationships within the code will perhaps give insight as to the specific action of calcium on the axoneme.

Chapter 2

Methods

2.1 The Geometric Clutch Hypothesis

Overview of cilia simulation Matlab code used for the original GCH.

The code first loads the parameter file to be used, specific to either a cilium or flagellum. The number of segments the cilium/flagellum is divided into is user-defined, and is typically set between thirty and sixty. When n segments are used, the following parameters are scaled accordingly: segment length, Ke, the elastic constant of nexin per segment, no. of dyneins per segment, and the scaling parameters listed in table 2.2 which are scaled linearly from their *best experimental value* at $n = 30$ (segments).

Table 2.1: Modeling Parameters for Cilia: Known from Experimental Value

	Cilium
Length (cm)	0.001
Diameter (cm)	1.0×10^{-5}
Iteration Interval (sec)	0.001
I_0E (passive stiffness of nexin) (dyne cm^2)	1.0×10^{-13}
Drag Coefficient (dyne cm^{-2} sec)	0.028
r (resting length of nexin) (cm)	3.0×10^{-6}
Z (segment length) (cm)	$\frac{0.001}{n}$
Ke (dyne/cm)	$\frac{Z}{1.0\times10^{-5}} \times 0.06$
No. of dyneins per segment	$Z \times 3.9 \times 10^6$

Table 2.2: Modeling Parameters for Cilia: Unknown

	Range	Best Constant Value
Transfer Coefficient	$0 \leq TC \leq 0.40$	0.14
Adhesion Scaling Factor	$30000 \leq ASF \leq 35000$	33000
T-Force Scaling Factor	$2000 \leq TFSF \leq 16000$	7000
B_P	$0 \leq B_P \leq 0.20$	0.06
B_R	$0 \leq B_R \leq 0.20$	0.01
Tug (force per dynein)	$3.0 \pm 2.0 \times 10^{-7}$	1.2×10^{-7}

Next, a separate function file updates the position of the cilium as well as the curvature and shear angles. The main iteration loop calculates both the passive and active forces acting along the axoneme. Within this loop, several variables are zeroed out at the beginning of each iteration. These variables inclue shear angle, curvature ($\frac{d\theta}{ds}$), longitudinal force, transverse force, t-force in the principal bend direction, t-force in the reverse bend direction, total torque, interdoublet shear (ds), and microtubule sliding velocity (all at each individual segment). Passive forces are generated by the action of the nexin links being stretched between the doublets as shown in figure 2.1. To calculate the passive longitudinal and transverse forces at each segment j (see figure 2.1), shear angle (ψ) and the angle of the stretched nexin (ϕ)

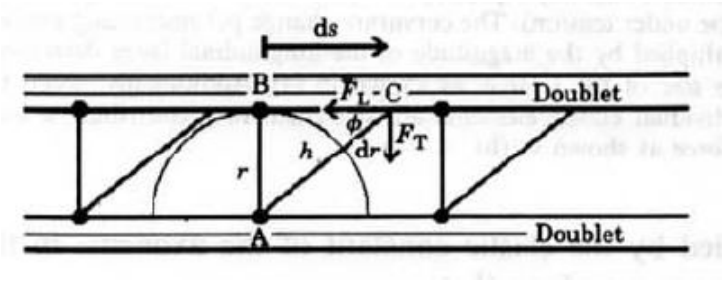

Figure 2.1: Passive forces are calculated from the nexin links between doublets: ds = interdoublet shear, ϕ = angle formed by nexin and doublet, dr = stretch of nexin, h = length of stretched nexin, r = resting length of nexin, F_L = longitudinal force component, F_T = transverse force component[9].

are passed to the following equations:

$$F_{L_j} = F_{E_j} \times cos\phi_j \times \frac{\psi_j}{|\psi_j|} \tag{2.1}$$

$$F_{T_j} = F_{E_j} \times sin\phi_j \tag{2.2}$$

where

$$F_{E_j} = Ke \times DR_j \tag{2.3}$$

$$DR_j = H_j - r \tag{2.4}$$

$$H_j = \sqrt{(\psi_j \times Diameter)^2 + r^2} \tag{2.5}$$

$$Ke = elastic\ constant\ of\ nexin\ (per\ segment)$$

$$r = resting\ length\ of\ nexin$$

.

In the above equations, (2.3) is the total elastic force exerted by the nexin links. The equation is derived from Hooke's law for a linear elastic spring, $F = kx$. Ke is the spring constant, and DR (2.4) is the displacement. In order to find the length of the stretched nexin, H, the Pythagorean theorem is used since the resting nexin forms a right angle with the plane of the doublet (see figure 2.1). To generate equations (2.1) and (2.2), F_E is multiplied by $cos\phi$ and $sin\phi$ for the longitudinal and transverse components, respectively. Equation (2.1) is also mulitplied by $\frac{\psi}{|\psi|}$ in order to capture the correct sign with respect to shear angle (i.e, which direction the microtubules are sliding). The pythagorean theorem is utilized in equation (2.5) to solve for H.

Next begins the active force calculations at each segment. The total t-force experienced at each segment j is the sum of both the passive forces contributed by the nexin links and the active force contributed by the dyneins. After summing the longitudinal t-forces from the tip towards the basal body (see figure 1.3), t-force in the principal and reverse bend directions at each segment j are calculated with the following equations:

$$T - Force_{P_j} = F_{T_j} + Z \times \frac{d\theta}{ds}_{j+1} \times P_{L_j} \tag{2.6a}$$

$$T - Force_{R_j} = F_{T_j} + Z \times \frac{d\theta}{ds}_{j+1} \times R_{L_j} \tag{2.6b}$$

where

$$P_{L_j} = \sum_{i=j}^{n} F_{L_j} + [F_{P_j} \times (1 - TC)] + [F_{R_j} \times TC] \tag{2.7a}$$

$$R_{L_j} = \sum_{i=j}^{n} F_{L_j} + [F_{R_j} \times (1 - TC)] + [F_{P_j} \times TC] \tag{2.7b}$$

$$TC = Transfer\ coefficient \tag{2.7c}$$

and

$$F_{P_j} = Tug \times D_{P_j} \tag{2.8a}$$

$$F_{R_j} = Tug \times D_{R_j} \tag{2.8b}$$

$$D_{P,R_j} = No.\ of\ engaged\ dynein\ bridges\ at\ segment\ j$$

In the above equations, F_{T_j} and F_{L_j} are the same as those in equations (2.1) and (2.2) and are responsible for contributing the passive transverse and longitudinal components of force, respectively. In equations (2.6a) and (2.6b), the curvature ($\frac{d\theta}{ds}$) is mulitplied by the segment length (Z) since both Z and ds are in units of length. P_{L_j} and R_{L_j} represent the forces that accumulate along the axoneme: when the cilium switches from the effective to the recovery stroke, some of the forces in the more distal end generated by the effective stroke are still felt by segments at the basal end during the recovery stroke. F_{P_j} and F_{R_j} (and in turn, P_{L_j} and R_{L_j}) are responsible for contributing the active components of force generated by the dyneins, and are calculated simply by multiplying the force

that one dynein generates by the total number of attached dyneins. With the ciliary beat divided into opposing principal and reverse bend directions, the active bending on one side of the axoneme generates a passive bending on the opposite side. For example, if all dyneins at segment j are engaged on the principal side (resulting in the active bending of the principal side), then it is likely that there will be little or no dyneins engaged at segment j on the reverse side. However, the reverse side still experiences a passive bending. These observations indicate that some of the force from dynein bridges on one side is "shared" with the opposite side. To account for this transfer of active force, F_{P,R_j} is mulitiplied by a transfer coefficient, TC, in equations (2.7a) and (2.7b). When calculating the active longitudinal forces in the principal bend (2.7a), the force of engaged dynein bridges on the principal side is multiplied by $1 - TC$ and the force of engaged dynein bridges on the reverse side is mulitplied by TC because the principal bend experiences most of the force from the principal side dyneins and only a little bit of the force from the reverse side dyneins[9].

The next step is to calculate how many dynein bridges should engage or "turn on" at each segment. This proved to be a challenge, since there are several different variables that must be taken into account in these calculations. Furthermore, little is known about what precisely regulates dynein activation or deactivation. Since one of the goals of this project is to propose a new, perhaps more biologically-based model of dynein regulation, two different models are explored and analyzed. The models differ in both the methods and variables used to calculate dynein attachment as well as the force generated by each dynein.

In the Geometric Clutch Hypothesis[9], dynein attachment is calculated using probabilities. T-forces are fed into equations that output adehsion probabilities. The idea is that when dynein bridges attach, they inherently pull the microtubule doublets closer together (decreasing the interdoublet spacing). This makes it easier for neighboring dyneins to attach, since the distance between the doublets has decreased. Resulting in a sort of "zipper" effect, the cascade of dynein attachment halts only when t-force is sufficiently strong[9].

To calculate the probability that dynein bridges will engage, an active probability is first formed by modifying the resting/base probability of attachment (B_P, B_R) to take into account the t-force:

$$P_{P_j} = B_P + (T - Force_{P_j} \times T - Force\ Scaling\ Factor) \tag{2.9a}$$
$$P_{R_j} = B_R + (T - Force_{R_j} \times T - Force\ Scaling\ Factor) \tag{2.9b}$$

where $B_{P,R}$ and the $T - Force\ Scaling\ Factor$ are set to values listed in table 2.2. Next, effects of adhesion are taken into account at each segment:

$$Adhesion_{P_j} = F_{P_j} \times Adhesion\ Scaling\ Factor \times (1 - P_{P_j}) \tag{2.10a}$$
$$Adhesion_{R_j} = F_{R_j} \times Adhesion\ Scaling\ Factor \times (1 - P_{R_j}) \tag{2.10b}$$

where F_{P,R_j} is the active force of engaged dynein bridges from (2.8a) and (2.8b) and the Adhesion Scaling Factor is a constant value listed in table 2.2. The scaling factor is necessary in order to obtain an adhesion value between 0 and 1 that is compatible with using probabilities[9]. In order to account for the "sharing" of the force effect discussed previously, the final equations for Adhesion are corrected with the $Transfer\ Coefficient$ listed in table 2.2 (the same $Transfer\ Coefficient$ is also used in eqns. (2.8) and (2.9)):

$$Adhesion_{P_j} = Adhesion_{P_j} - (TC \times Adhesion_{R_j}) \tag{2.11a}$$
$$Adhesion_{R_j} = Adhesion_{R_j} - (TC \times Adhesion_{P_j}) \tag{2.11b}$$

A dynamic probability is then used as a switch point within the active bridge loop and the loop is exited when there is less than a 10 percent change detected in dynein bridge attachment.

$$Dynamic_{P_j} = P_{P_j} + Adhesion_{P_j} + \frac{1}{2}Adhesion_{P_{j-1}} + \frac{1}{2}Adhesion_{P_{j+1}} \tag{2.12a}$$

$$Dynamic_{R_j} = P_{R_j} + Adhesion_{R_j} + \frac{1}{2}Adhesion_{R_{j-1}} + \frac{1}{2}Adhesion_{R_{j+1}} \tag{2.12b}$$

When working with either the first or last segment, the $j-1$ or $j+1$ term is dropped from the above equations (respectively).

After calculating dynein attachment, the active bridge loop is exited and the forces exerted by the dyneins are summed from the tip of the axoneme toward the basal body. This concludes the active force calculations.

Next, torque and equilibrium curvatures are calculated using information from passive and active force calculations. The total force and torque acting along each segment j is given by

$$F_{Total_j} = 2 \times \sum_{i=j}^{n} F_{L_j} + \sum_{i=j}^{n} F_{P_j} + \sum_{i=j}^{n} F_{R_j} \tag{2.13}$$

$$Torque_j = F_{Total_j} \times Diameter \tag{2.14}$$

After entering a drag loop to account for fluid viscocity, etc., the position of the cilium/flagellum is updated along with the shear angles and curvatures before beginning the next iteration.

Chapter 3

Analysis

3.1 Analyzing the Geometric Clutch Hypothesis

In order to better understand the essential factors that regulate ciliary and flagellar beating, the original Matlab model of the Geometric Clutch Hypothesis was critically analyzed.

In the Geometric Clutch model, curvature is defined as the difference of the angle formed by the nexin links and the microtubule at the jth segment and the j-1th segment .When curvature at the j^{th} segment is decreasing, the dyneins on the principle side are attached. Similary, when curvature is increasing, the dyneins on the reverse side are engaged. Local maximums and minimums in curvature also represent when opposing dyneins begin to turn on or off.

Shear angle is defined as the difference between the current angle formed by the j^{th} segment with the x-axis and the inital angle formed by the j^{th} segment with the x-axis. The cilium starts out in a straight vertical line along the y-axis, beginning at the origin (where it would be attached to a basal body) with the distal end furthest away. Given this starting position, the initial angle for all segments is 90^o. Therefore when shear angle at the j^{th} segment is decreasing, the j^{th} segment is moving in a clockwise direction through the first (and sometimes fourth) quadrant, and dyneins on the principle side are attached. Similary, when shear angle is increasing, the segment is moving in a counter-clockwise direction through the first and second quadrants, and dyneins on the reverse side are engaged. A local maximum or minimum in shear angle is typically coordinated with the switching point of the opposing dyneins. When shear angle is negative, the cilium is beating in mostly the first and some of the fourth quadrant (relative to the origin, where the basal body of the cell would be found). When shear angle is positive, the cilium is beating in the second quadrant.

Dyenin attachment is fairly coordinated in a normal cilium or flagellum. When dyneins on the principal (reverse) side are attaching, dyneins on the reverse (principal) side are either detaching or already detached (disengaged). Figure 3.1 shows this coordinated attachment (taken at a single time step). The "switching point" occurs when the t-force reaches a critical value. An episode of dynein attachment is propogated in part by the "zipper" effect as well as by the forces of adhesion discussed in section 2.1. The episode of attachment ends when t-force reaches a critical value to overcome to forces of adhesion generated by the dyneins.

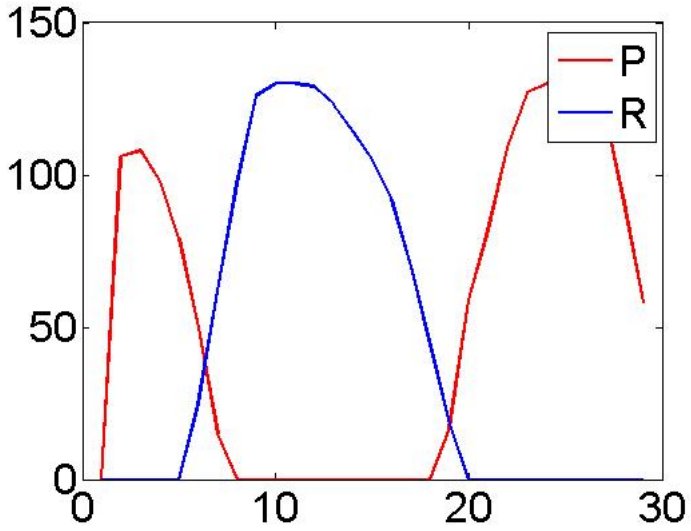

Figure 3.1: Dynein Attachment: segments 1-30 are shown along the x-axis, and the number of attached dyneins at each segment is shown along the y-axis. Once enough dyneins have detached from the principal side (shown in red), dyneins on the reverse side (shown in blue) begin to attach starting around the 5^{th} segment. The effect continues, and once the episode of attachment on the reverse side concludes, an episode of attachment on the principal side begins.

Microtubule sliding velocity is another important factor in ciliary and flagellar beating. It regulates, in part, the beat frequency. Sliding velocity is also useful in analyzing the effects of Ca^{2+} on cilia and flagella. When a cilium or flagellum arrests, the microtubule sliding velocity ($\frac{ds}{dt}$) is equal to zero. Hypothetically, then, sliding velocity should also be zero when the cilium switches from effective to recovery stroke or vice versa. A relationship exists between the sliding velocity and the force exerted by dynein. For example, if the cilium is in an arrested position, then perhaps dynein force should be at a maximum in order to prevent the microtubules (and cilium) from sliding/bending. One such relationship proposed by Lindemann[10] is shown in figure 3.2.

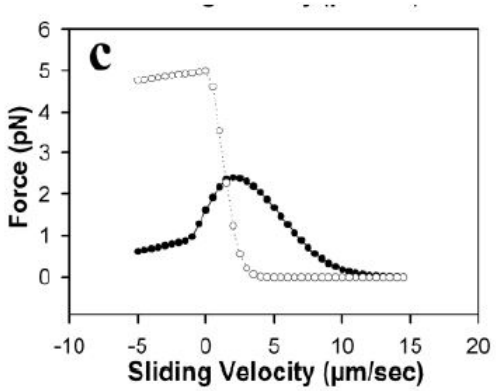

Figure 3.2: The force-velocity relationships proposed by Lindemann[10], where $force = f_0 e^{-(v-\alpha)^2 \times \beta}$, and α and β are modeling constants.

Some questions remain about how all the variables and parameters work together in the geometric clutch hypothesis to simulate ciliary beating. In an effort to better understand the roles of some of these parameters, an in-depth analysis of the model was completed. Altering one parameter at a

time, these changes were analyzed and compared to the orignal model using five key pieces of data: the time it takes to complete one beat, minimum and maximum curvature, minimum and maximum shear angle, dynein bridge engagement, and sliding velocity. Table 3.1 displays the results of changing some parameters.

Table 3.1: Changing Modeling Parameters
Baseline Parameters: Transfer Coefficient = 0.14, Adhesion Scaling Factor = 33000, T-Force Scaling Factor = 7000, Base P = 0.06, Base R = 0.01, Tug = 1.2×10^{-7}

Parameter Changed	Duration of One Beat (iterations)	Min Curvature	Max Curvature	Min Shear Angle	Max Shear Angle
Baseline	46	-7564	4625	-158.5	45.9
Transfer Coefficient = 0.07	33	-7349	4490	-145.6	51.5
Transfer Coefficient = 0.28	65	-8220	4568	-183.8	38.8
Adhesion Scaling Factor = 31000	35	-4726	1429	-140.3	11.1
Adhesion Scaling Factor = 35000	50	-9170	5760	-201.3	48.5
T-Force Scaling Factor = 3500	71	-9122	4178	-197.0	33.0
T-Force Scaling Factor = 14000	31	-5706	5824	-126.7	62.8
Base P = 0.06 Base R = 0.06	40	-7412	6257	-89.4	94.1
Tug = 1.4×10^{-7}	50	-16765	7478	-254.7	66.1
Tug = 1.6×10^{-7}	>100	-14541	8519.7	-370.0	111.2

While there were several parameter changes that resulted in interesting results, three were chosen to highlight some of the key pieces of the geometric clutch puzzle. These include changing the transfer coefficient from 0.14 to 0.07, changing the base switching probability for the reverse bend from 0.01 to 0.06 (to be equal to the base switching probability for the principal bend), and changing the t-force scaling factor from 7000 to 3500. These parameters are defined in the context of the GCH in 2.1.

An excellent overall indicator of how the cilium or flagellum is beating is the waveform generated by the simulation. Figure 3.3 shows the effects of changing the three parameters described above. At the baseline (3.3 (A)), with no parameter values changed, the cilium beats mostly in the first and second quadrants and has distinct effective and recovery strokes. With the transfer coefficient changed from 0.14 to 0.07 (3.3 (B)), the cilium still beats in mostly the first and second quadrants but is slightly more in the second quadrant than the baseline. When the base probabilities for random chance of dynein attachment are equal for the principal and reverse bends (3.3 (C)), the cilium beats noticeably more symmetrically about the y-axis. It also is less distinct in which direction the effective and recovery strokes go. The cilium also never beats below the x-axis, but the maximum y-value attained is noticeably greater. When the t-force scaling factor is changed from 7000 to 3500 (3.3 (D)), the cilium beats almost entirely in the first and fourth quadrants, with much sharper curves seen along the length of the cilium. The sharper bending results in the cilium beating more oftenly below the x-axis, and the maximum y-value attained is smaller. In the recovery stroke, it does not attain the maximum shear angle that is attained when it is set at the baseline, i.e. it does not go as far into second quadrant.

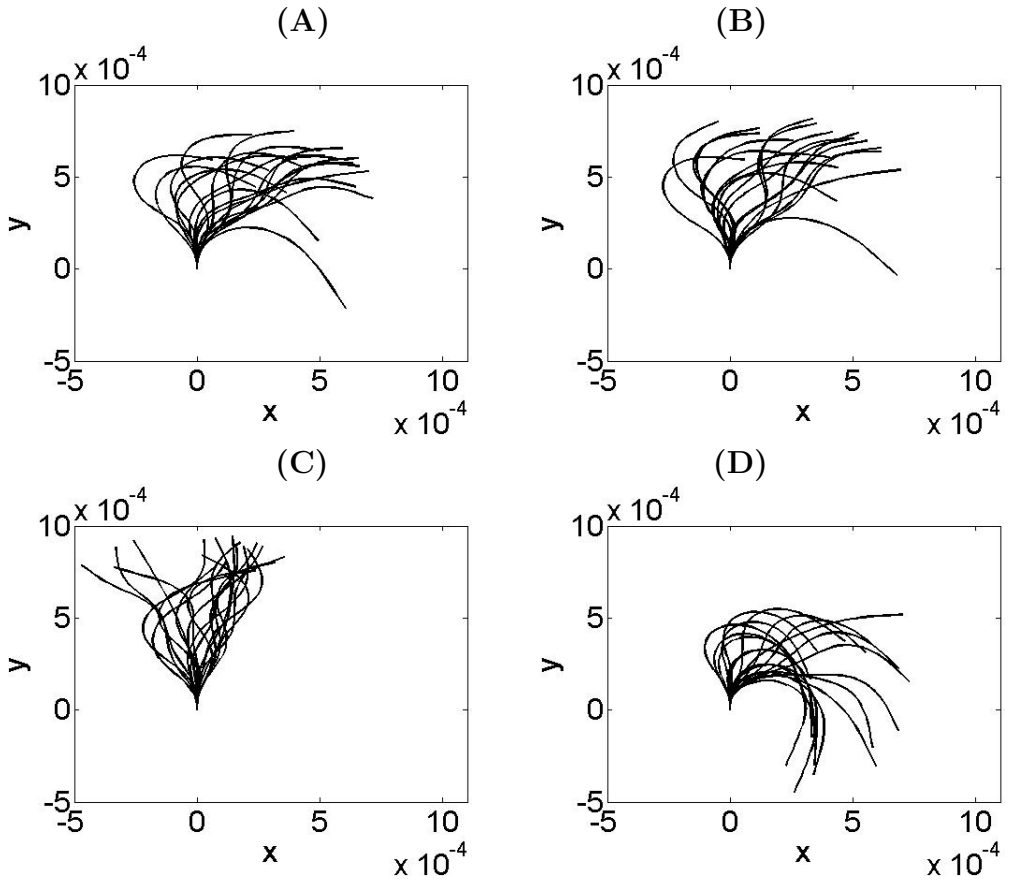

Figure 3.3: Waveforms: (A) is baseline, (B) is Transfer Coefficient = 0.07, (C) is $\text{Base}_P = \text{Base}_R = 0.06$, (D) is T-Force Scaling Factor = 3500. Note how location of beatform in quadrants I-IV varies and indicates the asymmetry of the beat. The maximum and minimum y-values attained by any segment of the cilium also varies with parameter changes.

Another key indicator for comparison is curvature. In figure 3.4, the x-axis respresents time (going from 0 to 100 milliseconds) and the y-axis represents segments along the axoneme, where segment one is closest to the basal cell body and segment thirty is the most distal (furthest from the basal body). The shading represents the curvature, where red indicates maximal curvature, yellow indicates zero curvature, and blue indicates minimal curvature. The graphs above show a clear propogation of a wave traveling down the cilium. In the baseline case, the two red protrusions represent this active wave. They are an excellent indicator of ciliary beat frequency- how fast the cilium is beating. When run for 100 iterations, the cilium makes two clear beats when all parameters are set at their baseline values (3.4 (A)). A maximum or a minimum in curvature represents when the principal and the reverse bend dyneins begin to "switch". When the transfer coefficient is set at half of its original value (3.4 (B)), the cilium makes nearly three beats within 100 iterations, indicating that decreasing the transfer coefficient increases the beat frequency of the cilium. Since local maximums and minimums are closer together, the dyneins are acting faster. As noted in table 3.1, in a coordinated manner, when the transfer coefficient is set at double its original value, the cilium only makes one clear beat. When the baseline probabilities of a spontaneous switching of dyneins from the principal bend to the reverse bend or vice versa are set to be equal, as in 3.4 (C), curvature propagates down the entire length of the cilium. What makes (C) so strikingly different from the others is the positive curvature found in

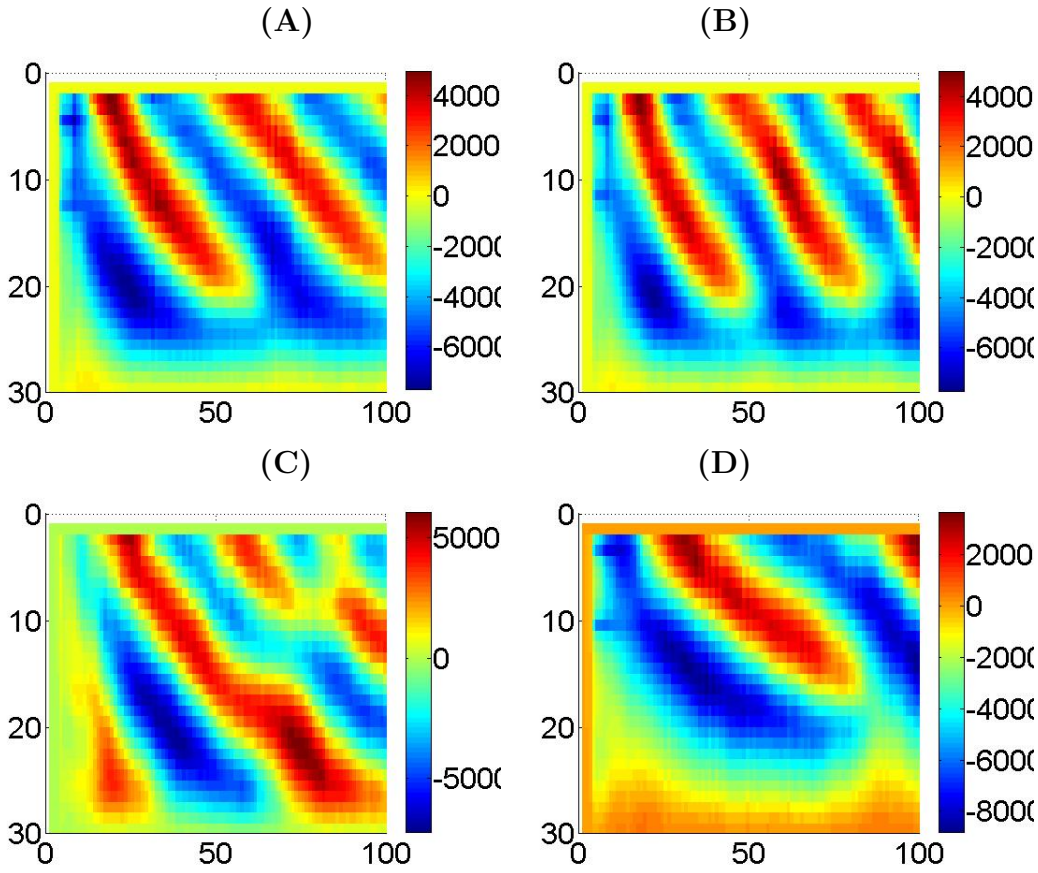

Figure 3.4: Curvature: (A) is baseline, (B) is Transfer Coefficient = 0.07, (C) is $\text{Base}_P = \text{Base}_R = 0.06$, (D) is T-Force Scaling Factor = 3500. Note the variation in both the size and location of the red colored areas (positive curvature) versus the blue colored areas (negative curvature).

the distal segments. Since the cilium beats more symmetrically when these probabilities are equal, the cilium bends in both directions with equal favor, and so the curvature is seen as more evenly distributed. One last interesting case to look at is the t-force scaling factor set to half of its original value (3.4 (D)). Not only does the cilium ony make one beat,but the wave does not reach the more distal segments at all.

Shear angles fill in another important piece of the puzzle when it comes to the regulation of dyneins in cilia and flagella. In figure 3.5, the x-axis again represents time (going from 0 to 100 milliseconds) and the y-axis respresents shear angle (in degrees). Shear angle was tracked at the 5^{th} (shown in red), 10^{th} (shown in blue), 15^{th} (shown in green), 20^{th} (shown in yellow), and 25^{th} (shown in black) segments. As noted previously, a maximum or a minimum in shear angle represents when the cilium switches between the effective and recovery strokes. When shear angle is decreasing, the cilium is in the effective stroke, and when shear angle is increasing, the cilium is in the recovery stroke. The amplitude of the waves in the shear angle plots tell how far from the cilium's starting position (90^o) the cilium travels (i.e, how "broad" of a sweep the cilium makes). When the transfer coefficient is set to 0.07 (3.5 (B)), the shear angle plot looks as if it is simply a copy of (A) with a higher frequency. Though not pictured, the graph of shear angle when the transfer coefficient is doubled from 0.14 to 0.28 looks the opposite: similar to (A) if it were more "stretched out," with a decrease in frequency, indicating a decrease in ciliary beat frequency. In 3.5 (C), when the base resting probability of a

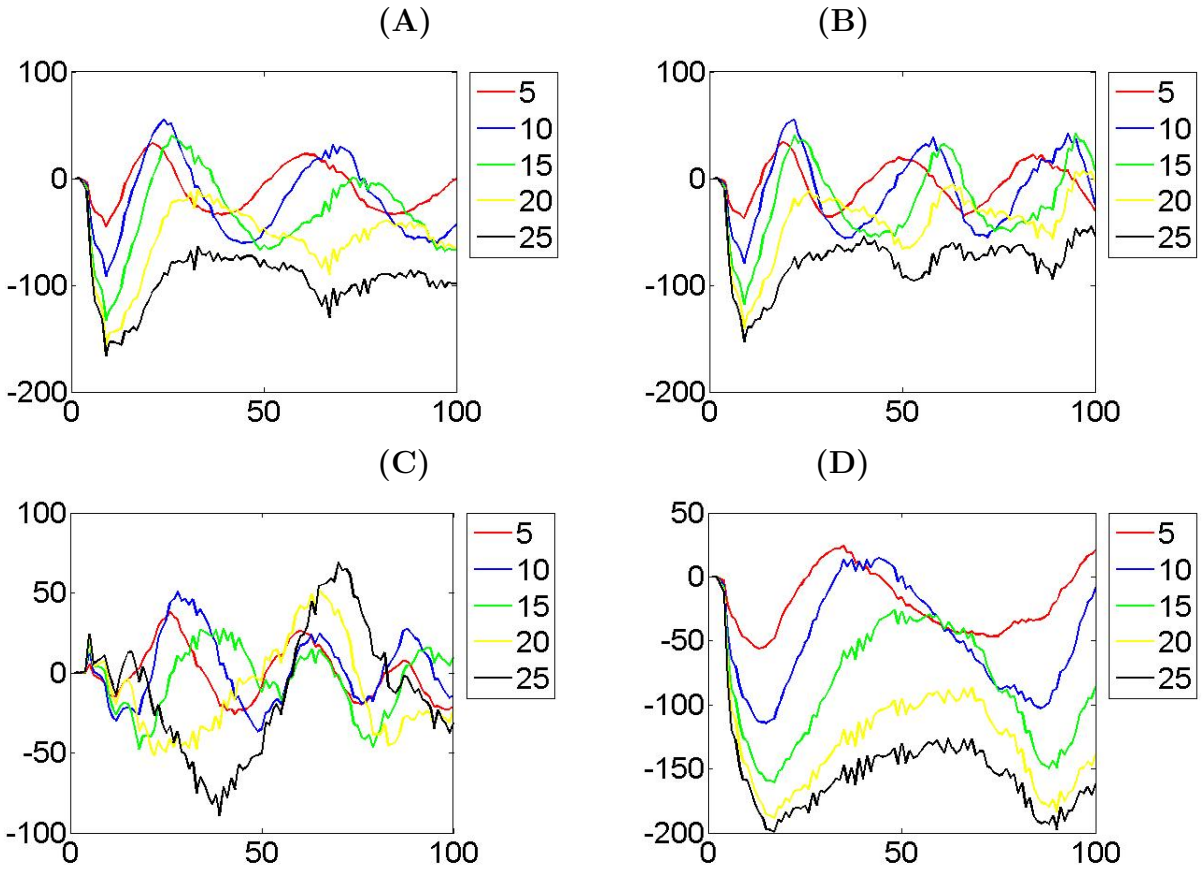

Figure 3.5: Shear Angle: (A) is baseline, (B) is Transfer Coefficient = 0.07, (C) is $\text{Base}_P = \text{Base}_R = 0.06$, (D) is T-Force Scaling Factor = 3500. Note the variation in both frequency and amplitude of the "waves".

dynein "switching" is equal for the principal and reverse bends, the cilium beats more symmetrically. Since a shear angle of zero indicates a return to the initial starting position (the y-axis), the even distribution of local maximums and minimums across the x-axis signal the even distribution of beating in the first and second quadrants. When the t-force scaling factor is set to half of its original value (3.5 (D)), the cilium is beating in primarily the first and fourth quadrants, and is getting "stuck" to bending in one direction. Ciliary beat frequency also decreases with a decrease in the t-force scaling factor.

Dynein attachment at the baseline parameters is coordinated: as dyneins on the principal bend begin to attach, dyneins on the reverse bend begin to detach and vice versa. In the graphs in figures 3.6 and 3.7, the x-axis once again represents time (going from 0 to 100 milliseconds) and the y-axis represents segments, with segment one being closest to the basal body (or the origin in figure 3.3) and segment thirty being the furthest. The color bar indicates how many dyneins are engaged at each segment: red represents maximal dynein attachment (i.e, when all dyneins in a given segment are attached) and blue represents minimal dynein attachment (with zero meaning that no dyneins are attached). When the cilium is divided up in to thirty segments, there are 130 dyneins on each segment. For example, if 80 out of 130 dyneins on segment j are attached on the principal side, then there will be $\leq$50 dyneins attached on segment j on the reverse side (see figure 3.1: dynein attachment at a single time step). When run for 100 iterations, 3.6 (A) and 3.7 (A) show dynein attachment

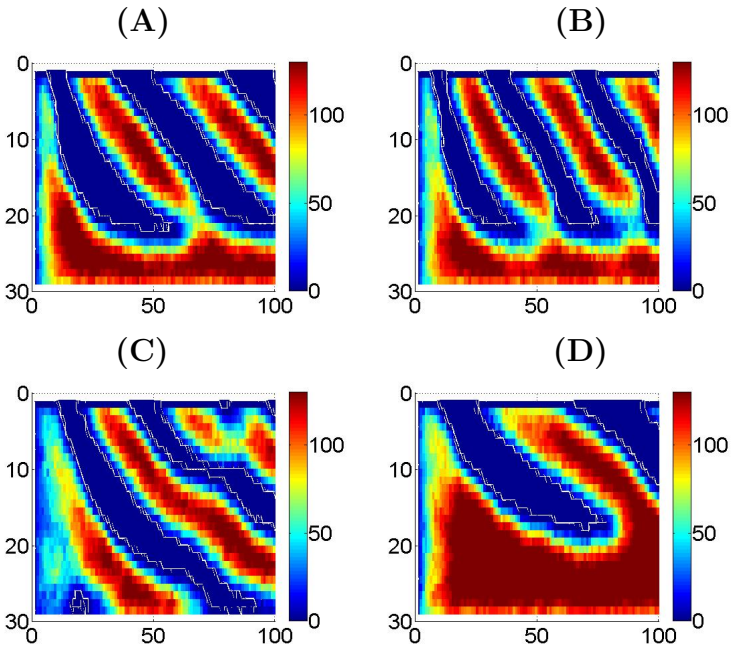

Figure 3.6: Dyneins P: (A) is baseline, (B) is Transfer Coefficient = 0.07, (C) is $\text{Base}_P = \text{Base}_R = 0.06$, (D) is T-Force Scaling Factor = 3500

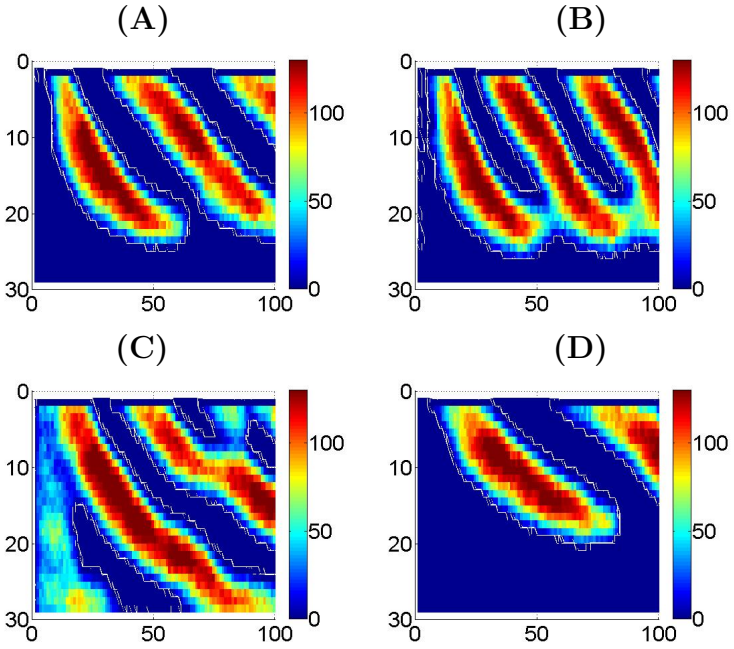

Figure 3.7: Dyneins R: (A) is baseline, (B) is Transfer Coefficient = 0.07, (C) is $\text{Base}_P = \text{Base}_R = 0.06$, (D) is T-Force Scaling Factor = 3500

for approximately two full beats. When the transfer coefficient is set to half of its original value, the dyneins turn on and off more quickly so the cilium makes one more fullbeat than when set at the baseline parameters (3.6 (B) and 3.7 (B)). When the baseline probabilites of a dynein switching are equal, the wave again propagates down the entire length of the axoneme, with even the more distal

segments fully engaging and disengaging dyneins (3.6 (C) and 3.7 (C)). In figures 3.6 (D) and 3.7 (D), when the t-force scaling factor is only half that of its original value, the dyneins on the more distal segments are always on in the principal bend, and the dyneins in the reverse bend don't turn on at all. This is perhaps due to the lack of t-force felt at the distal ends, since t-force is summed from the distal ends to the basal end segments. This means the segments at the end of the cilium (segments 20-30) have not accumulated enough t-force to engage a full "switch" in the bend.

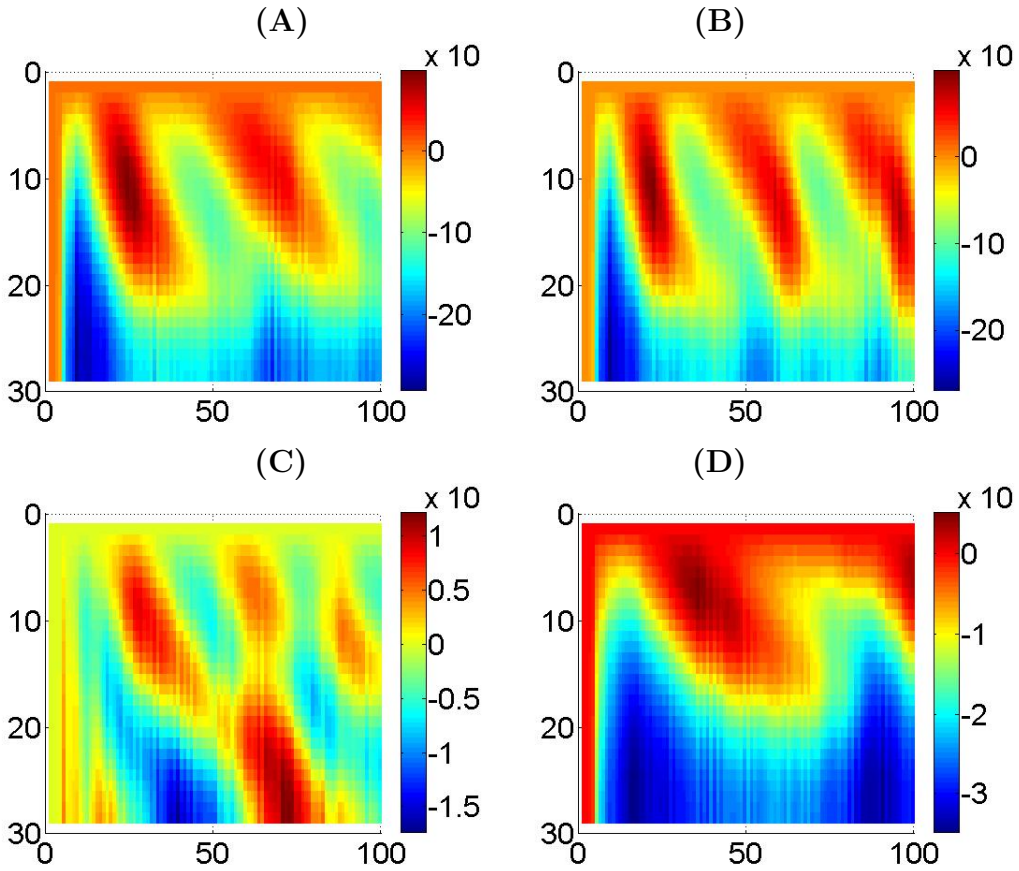

Figure 3.8: Sliding Velocity (ds/dt): (A) is baseline, (B) is Transfer Coefficient = 0.07, (C) is Base$_P$ = Base$_R$ = 0.06, (D) is T-Force Scaling Factor = 3500

Sliding velocity is a key indicator of ciliary beat frequency and the "switch point" when the cilium switched from effective to recovery stroke or vice versa. Figure 3.8 shows the effects of varying parameter values on sliding velocity. The x-axis represents time (0-100 milliseconds) and the y-axis represents segments j from 1 to 30. When all parameters are set to their basline values, as in 3.8 (A), the cilium makes two clear beats, and sliding velocity ranges from about -25×10^{-3} to 10×10^{-3} centimeters per millisecond. When the transfer coefficient is set to half of its original value (3.8 (B)), the cilium makes three clear beats, with sliding veloctities on the same range as 3.8 (A). In 3.8 (C), when the baseline probabilities are equal, there is an overall decrease in the magnitude of sliding velocity. Sliding velocity is also near zero more often, and the ciliary "beat" is unclear. However, noticeably different in (C) is the positive sliding velocity acheived by more distal segments ($20 \leq j \leq 30$) that is not present in any of (A), (B), or (D). When the t-force scaling factor is set to 3500, as in 3.8 (D), the cilium makes only one clear beat, and an overall decrease in the magnitude of sliding velocity is apparent. As previously stated, sliding velocity should be close to zero when

the cilium makes a switch from effective to recovery stroke or vice versa. However, based on the comparison of figures 3.8 and 3.5, it is clear that in the case of the GCH, a minimum in sliding velocity (occurring at the same time as a minimum in shear angle) indicates a switch from effective to recovery stroke. Likewise, a maximum in sliding velocity (occurring at the same time as a maximum in shear angle) indicates a switch from recovery to effective stroke.

Chapter 4

The Challenge

4.1 A Varying Dynein Force

The challenge in the project lies in defining the force that each dynein can generate. The original code provided a constant value for the force exerted by each dynein ($Tug = 1.2 \times 10^{-7}$ dyne)[9]. However, it is now known that the force generated by each dynein can vary greatly. With this knowledge, an ordinary differential equation for the value of Tug in both the principal and reverse bend directions was implemented based on the microtubule sliding velocity.

Measurements of the stall force of dynein have greatly varied in experiments previously performed. One such example is the third version of the geometric clutch hypothesis, in which the outer and inner dynein arms pull with different forces based on microtubule sliding velocity. After passing sliding velocity to either a Guassian or a linear function for the inner and outer arms, respectively, dynein force is calculated. In Lindemann's Geometric Clutch Version Three[10], the force the dyneins are capable of generating is given by a modified version of Charles Brokaw's[4] Gaussian relationship

$$Force = F_0 e^{-(v-\alpha)^2 \times \beta} \tag{4.1}$$

where v is the sliding velocity and α, β are modeling constants determined by best fit. In our model modified from the original GCH, sliding velocity at the jth segment can be calculated as

$$v_j = \frac{ds_j}{dt} \tag{4.2}$$

where ds is the distance the microtubule has moved (see figure 2.1: interdoublet shear) and dt is the time step being used (iteration interval). Since the model uses time step dt=0.001 seconds, velocity can be calculated as $v_j = \frac{ds_j}{0.001}$. In equation (4.1), since the force is dependent upon time, one can compare it to the general, well-known equation for population growth $P = P_0 e^{rt}$. The population at time t is given by an exponential growth equation where P_0 is the initial population at time $t = t_0$ (initial time, e.g. $t = 0$) and r is the growth rate of the population. Since $\frac{dP}{dt} = rP$, using this framework, one can begin to think of Tug as an ordinary differential equation (time-varying on each segment). Drawing upon these aspects, the following ODEs for Tug were generated:

$$\frac{dTug_{P_j}}{dt} = -k_1 \times f(v_j) \tag{4.3a}$$

$$\frac{dTug_{R_j}}{dt} = k_1 \times f(v_j) \tag{4.3b}$$

where k_1 is a modeling constant determined by best fit and $f(v_j)$ is the velocity term.

Once given an initial condition (an initial Tug value), equations (4.3a) and (4.3b) can be handled as an ordinary first-order differential equation. For example, when $\frac{dTug_{P,R_j}}{dt} = 0$, Tug is constant, which is the case as in the original Geometric Clutch Hypothesis[9]. As sliding velocity (v_j) decreases, the change in Tug also decreases: when the cilium is beating very slowly (i.e. v_j small), the dyneins are pulling with a constant force.

In order to implement (4.3a) and (4.3b), the Euler method was used. Since the sliding velocity at each segment is known, it is treated as a constant. First, let us write the equation in a format more suitable to implement Euler:

$$y'_P = -k_1 \times f(v) \tag{4.4a}$$
$$y'_R = k_1 \times f(v) \tag{4.4b}$$
$$y_0 = 1.2 \times 10^{-7}$$

where y' is the change in Tug, v is the sliding velocity, and y_0 is the initial condition at iteration $n = 0$ for both the P and R bend directions. The Euler method uses the following equation to calculate the next value of y (Tug):

$$y_{n+1} = y_n + hf_n \tag{4.5}$$

where h is the step size and f_n is the function given by y' (in this case, equations (4.4a) and (4.4b)). Taking n to be the iteration, j to be the segment number, and setting h=0.001 seconds, we have:

$$y_{P_{j_{n+1}}} = y_{j_n} - 0.001 \times k_1 \times f(v_{j_n}) \tag{4.6a}$$
$$y_{R_{j_{n+1}}} = y_{j_n} + 0.001 \times k_1 \times f(v_{j_n}) \tag{4.6b}$$

Now, in order to implement this ODE into the Matlab code, two separate equations were used for Tug in the principal and reverse bend directions. Resuming our Matlab terminology from 2.1, we have:

$$TugP_{j_n} = TugP_{j_{n-1}} - 0.001 \times k_1 \times f(v_{j_n}) \tag{4.7a}$$
$$TugR_{j_n} = TugR_{j_{n-1}} + 0.001 \times k_1 \times f(v_{j_n}) \tag{4.7b}$$

with

$$0.0 \leq k_1 \leq 0.9$$

The choice to use opposite signs for k_1 in (4.7a) to a + sign in (4.7b) was made in order to account for the "sharing" of the force of dyneins discussed in section 2.1. If Tug on the principal side is decreasing, then Tug on the reverse side should, in theory, be increasing in order to account for the force lost in the principal bend. Using 1.2×10^{-7} dyne as an initial value for both the principal and reverse sides ($TugP, R_{j_0} = 1.2 \times 10^{-7}$), the equation can be solved to update Tug at each iteration.

Four different sliding velocity terms ($f(v_j)$) were tested:

1. $f(v_j) = v_j^2$ with $0.01 \leq k_1 \leq 0.08$
2. $f(v_j) = v_j^3$ with $0.1 \leq k_1 \leq 1.00$
3. $f(v_j) = (v_j - v_0)^2$ with $0.01 \leq k_1 \leq 0.05$

4. $f(v_j) = (v_j - v_0)^3$ with $0.1 \leq k_1 \leq 1.00$

where v_0 is a critical value of sliding velocity.

As noted by Charles Lindemann[11], the sliding velocity is very close to zero when the cilium or flagellum reaches a "switch point" in bend direction. Since a maximum or minimum in shear angle indicates a switch from effective to recovery stroke (and vice versa), this is when dynein force should be greatest[11]. As sliding velocity increases, the force per dynein head should decrease.

Results from running simulations implementing the above equation for the force of dyneins are given in table 4.1.

Table 4.1: The Effects of Varying Dynein Force
Baseline Parameters: $TugP, R_j(0) = 1.2 \times 10^{-7}$ dyne per dynein for all j, $v_0 = -0.0050$ (average sliding velocity)

$f(v_j) =$	k_1	Duration of One Beat (iterations)	Min Sliding Velocity	Max Sliding Velocity	Min Tug	Max Tug
v_j^2	0.05	52	-0.0190	0.0076	0	1.3798×10^{-7}
v_j^3	0.40	42	-0.0341	0.0092	0	1.3587×10^{-7}
$(v_j - v_0)^2$	0.03	50	-0.0243	0.0096	0	1.3114×10^{-7}
$(v_j - v_0)^3$	1.00	42	-0.0394	0.0087	0	1.6082×10^{-7}

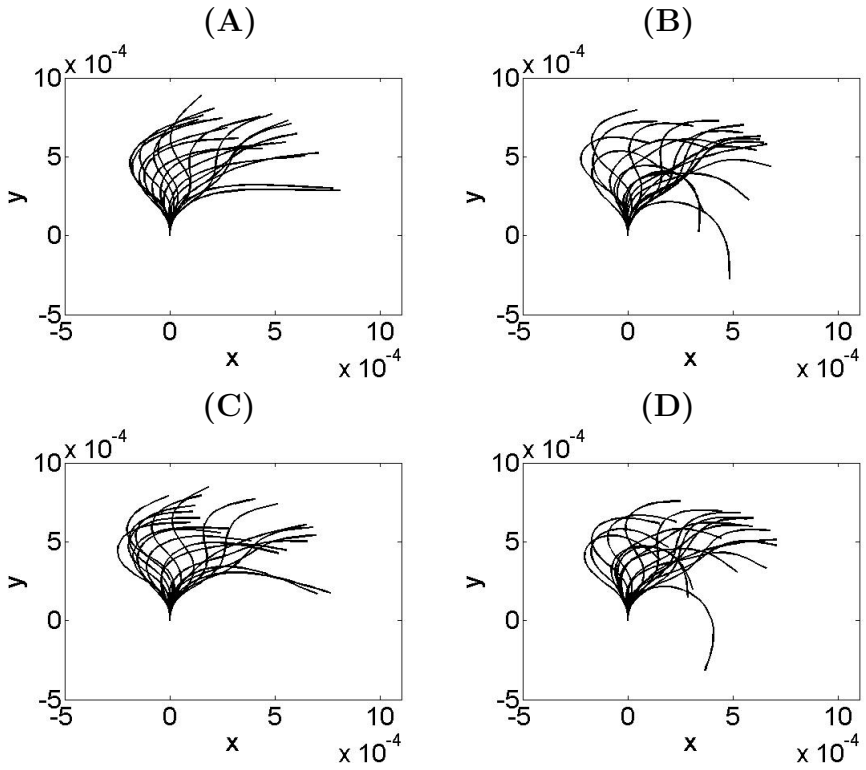

Figure 4.1: Varying Dynein Force - Waveforms: (A) $f(v_j) = v_j^2$, $k = 0.05$ (B) $f(v_j) = v_j^3$, $k = 0.40$ (C) $f(v_j) = (v_j - v_0)^2$, $k = 0.03$ (D) $f(v_j) = (v_j - v_0)^3$, $k = 1.00$

Figure 4.1 shows different beatforms as a result of varying the velocity terms in equations (4.7a) and (4.7b). When $f(v_j) = v^2$, as shown in figure 4.1 (A), the cilium beats noticeable more "stiffly".

It beats primarily in quadrant one, and the distal half of the cilium is mostly straight. Though the beatforms are not shown, it is notable to mention that as the value of k is decreased towards zero, the range of the effective stroke of the cilium increases (i.e. begins to beat in quadrant two as well) and the bending (curvature) of the cilium increases. When k is set to values above 0.08, the cilium begins to twist sharply before coiling up, and the simulation halts. When $f(v_j) = v^3$ and k=0.40, as in figure 4.1 (B), the cilium beats in a similar manner to that of the original GCH. In (C), the average (mean) sliding velocity is subtracted from the current sliding velocity before the term is squared. The effects are an increase in curvature, compared to that seen in (A), as well as a broader beatform. These effects are similar when the average (mean) sliding velocity is subtracted from the current sliding velocity and cubed, as in figure 4.1 (D).

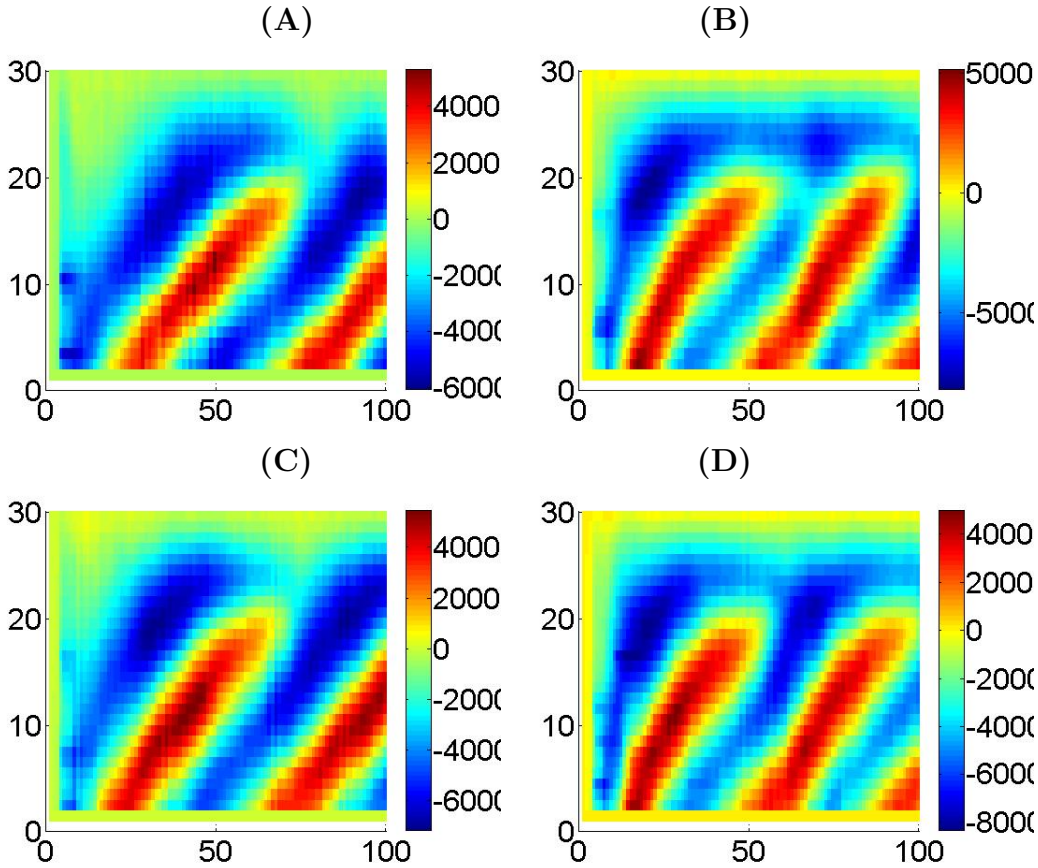

Figure 4.2: Varying Dynein Force - Curvature: (A) $f(v_j) = v_j^2$, $k = 0.05$ (B) $f(v_j) = v_j^3$, $k = 0.40$ (C) $f(v_j) = (v_j - v_0)^2$, $k = 0.03$ (D) $f(v_j) = (v_j - v_0)^3$, $k = 1.00$

As previously stated, curvature is an excellent measure of how sharply the cilium is bending. Figure 4.2 shows curvature for four different velocity terms, with the x-axis representing time (100 iterations at 0.001 sec/iteration) and the y-axis representing segments, j. When the velocity term is raised to the power two, as in 4.2 (A) and (C), the more distal segments ($j > 20$) remain fairly straight. These segments spend much more time at near-zero curvature (represented by the pale green color) than the same segments in 4.2 (B) and (D). When the velocity term is raised to the power three, as in (B) and (D), the cilium bends more at the distal ends and also makes two clear, complete beats.

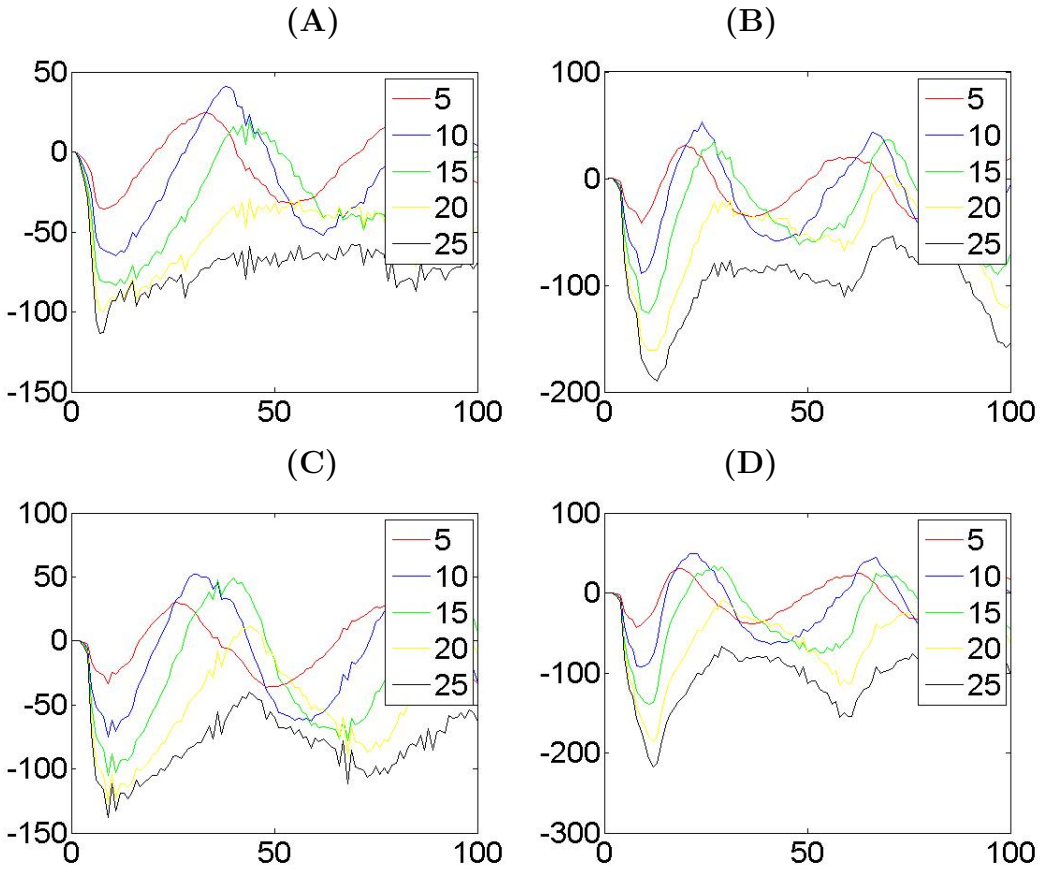

Figure 4.3: Varying Dynein Force - Shear Angle: (A) $f(v_j) = v_j^2$, $k = 0.05$ (B) $f(v_j) = v_j^3$, $k = 0.40$ (C) $f(v_j) = (v_j - v_0)^2$, $k = 0.03$ (D) $f(v_j) = (v_j - v_0)^3$, $k = 1.00$

Shear angle is a measure of the change in angle from the cilium's initial position (along the y-axis at x=0) to it's current position. Figure 4.3 shows shear angle plots for the four different velocity terms used. The x-axis represents time (0-100 milliseconds) and the y-axis represents shear angle measured in degrees. When the velocity term is chosen to be squared, as in 4.3 (A) and (C), the cilium's range of motion is decreased. The maximum shear angle achieved is noticeably smaller than that of 4.3 (B) and (D), indicating that the cilium does not move as far into the second quadrant (when shear angle is positive) when using a velocity squared term. Similarly, the minimum shear angle acheived in (A) and (C) is smaller in magnitude than that of (B) and (D), meaning that the cilium does not move as far into the fourth quadrant. Since a minimum in shear angle represents when the cilium switches from effective to recovery stroke, it is also apparent that the cubed velocity terms in figure 4.3 (B) and (D) result in an increased ciliary beat frequency. (B) and (D) attain more local minimums than that of (A) and (C), and therefore the cilium is beating faster.

Figures 4.4 and 4.5 show the Tug values calculated using equations (4.7a) and (4.7b). Dynein force (Tug) is plotted along the y-axis versus time along the x-axis at five evenly-spaced segments. In 4.4 (A) and (C), when the velocity term is squared, the Tug force changes rapidly at the more distal ($20 \leq j \leq 30$) segments. Furthermore, when $f(v_j) = v_j^2$, the maximum Tug force attained is about 1.38×10^{-7} (see 4.5 (A)). In comparison, when $f(v_j) = v_j^3$, the maximum Tug force attained is about 1.35×10^{-7}. Though the Tug values of 4.5 (A) are on the same range as those of 4.4 (B), the corresponding beatforms are strikingly different (see figure 4.1 (A) and (B)). When $f(v_j) = (v_j - v_0)^3$,

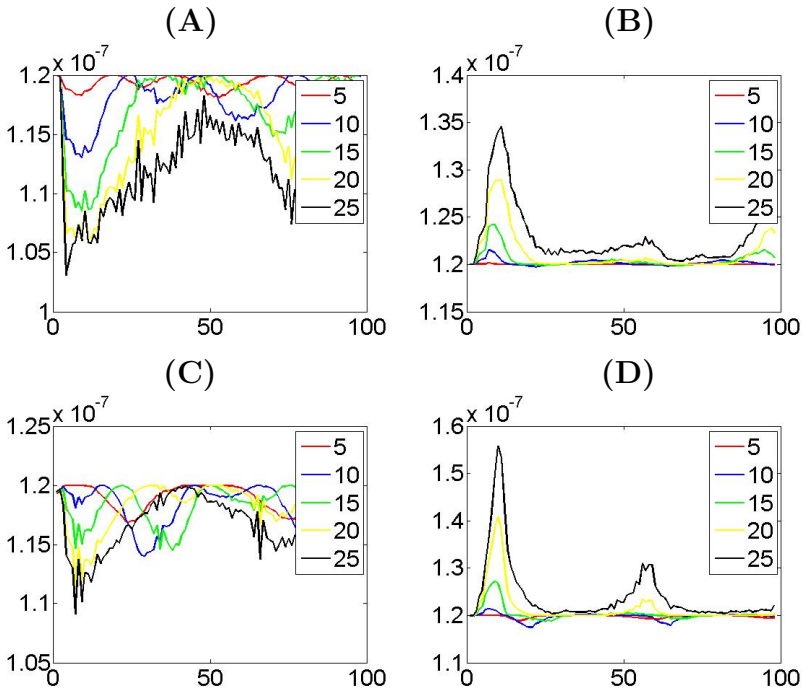

Figure 4.4: Varying Dynein Force - Principal Tug: (A) $f(v_j) = v_j^2$, $k = 0.05$ (B) $f(v_j) = v_j^3$, $k = 0.40$ (C) $f(v_j) = (v_j - v_0)^2$, $k = 0.03$ (D) $f(v_j) = (v_j - v_0)^3$, $k = 1.00$

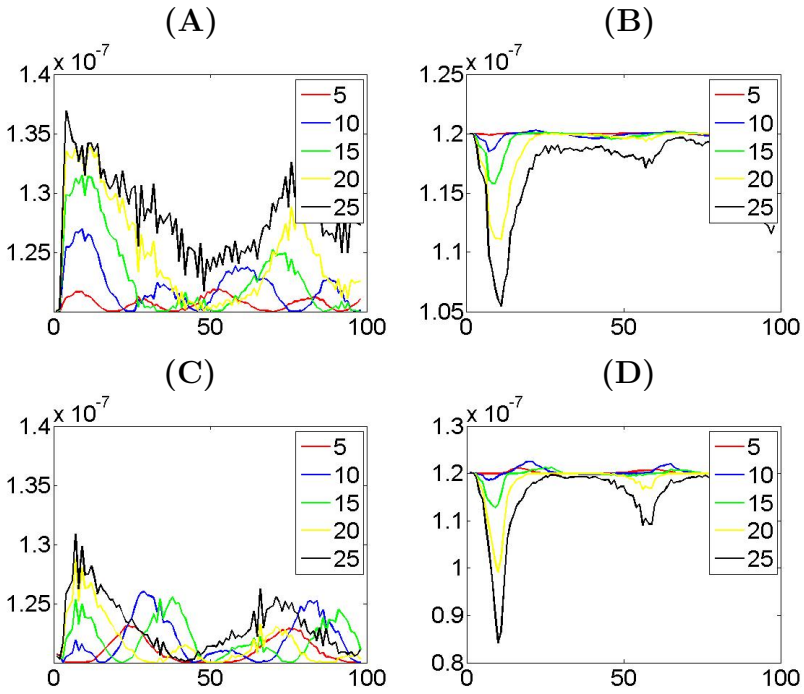

Figure 4.5: Varying Dynein Force - Reverse Tug: (A) $f(v_j) = v_j^2$, $k = 0.05$ (B) $f(v_j) = v_j^3$, $k = 0.40$ (C) $f(v_j) = (v_j - v_0)^2$, $k = 0.03$ (D) $f(v_j) = (v_j - v_0)^3$, $k = 1.00$

as in 4.4 (D), the maximum Tug force attained is around 1.6×10^{-7}. This could account for the slight

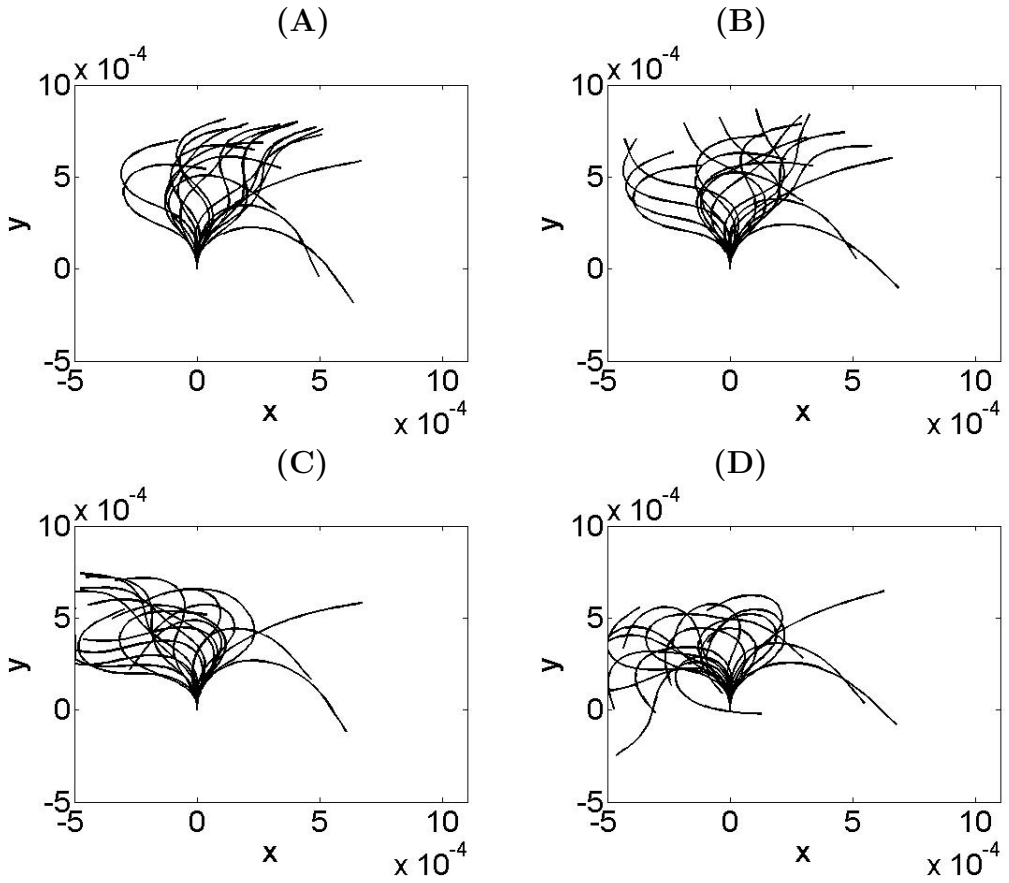

Figure 4.6: Varying Dynein Force Waveforms with $f(v_j) = (v_j - v_0)^3$, v_0 = -0.0300 (average minimum sliding velocity): (A) k=0.06, (B) k=0.08, (C) k=0.10, (D) k=0.15

increase in curvature seen in 4.1 (D).

After running numerous simulations using the different functions $f(v_j)$, the decision was made to further investigate the effects of implementing $f(v_j) = (v_j - v_0)^3$. Three different values of v_0 were used: v_0 = average sliding velocity, v_0 = average minimum sliding velocity, and v_0 = average maximum sliding velocity. Varying values of k_1 were used for each v_0 value.

Figure 4.6 shows the results of setting v_0 equal to an average minimum sliding velocity of -0.0300. When k is set to 0.06 (4.6 (A)), the cilium beats mostly in the first quadrant and barely in the second. The maximum value of Tug for (A) was 1.2428×10^{-7}, which is hardly a change from its initial value of 1.2000×10^{-7}. In striking contrast however, when k is set to 0.08 (4.6 (B)), the cilium beats noticeably broader. It extends further into the second quadrant, and exhibits a wide range of motion. Interestingly enough, the maximum value of Tug for (B) was 1.2684×10^{-7}. While the change in Tug is still relatively quite small, the differences in the overall beatform from (A) to (B) are readily apparent. This effect continues as the value of k is increased. When k is set to 0.10, as in 4.6 (C), the cilium beats primarily in the second quadrant. This is perhaps a result of the decrease in range of the recovery stroke (and an increase in range of the effective stroke). Since the effective stroke is broader than that of 4.6 (A) and (B), it takes the cilium further to the left. As a result, the range of the recovery stroke is minimized. An increase in curvature is also seen in both (C) and (D). When k is set to 0.15, as in 4.6 (D), the maximum curvature attained is on the range of 11,000, compared to a maximum curvature on the range of 9,000 in (C), 6,000 in (B) and 5,000 in (A). In 4.6 (D), k is set to

the maximum value that produces a working simulation. Though the maximum Tug exerted is still $< 2.0\times10^{-7}$, the cilium exhibits sharp bends and primarily beats in the second quadrant. It should also be noted that when running the simulation with $k = 0.15$, it became difficult to keep track of the effective and recovery strokes due to an increase in the propagation of bending down the axoneme (i.e. the more distal segments were still "bent" from the recovery stroke when the cilium began it's effective stroke).

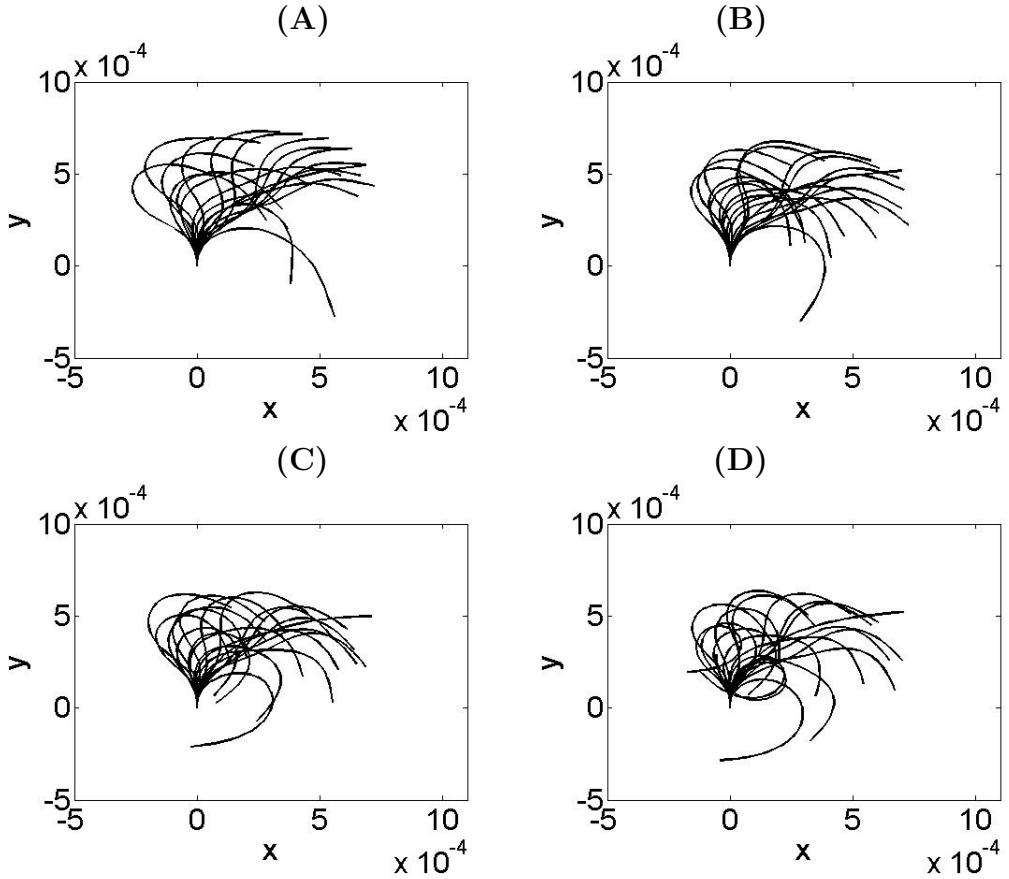

Figure 4.7: Varying Dynein Force Waveforms with $f(v_j) = (v_j - v_0)^3$, $v_0 = 0.0090$ (average maximum sliding velocity): (A) k=0.10, (B) k=0.20, (C) k=0.40, (D) k=0.45

Figure 4.7 shows the results of implementing $f(v_j) = (v_j - v_0)^3$ with $v_0 = 0.0090$, an average maximum sliding velocity. When k is set to 0.10, as in 4.7 (A), the beatform of the cilium is similar to the beatforms generated by the original GCH. Since the maximum value of Tug generated is only 1.2727×10^{-7}, the beatform is consistent with what one would expect for very slight variations in Tug. When k is set to 0.20, as in 4.7 (B), the cilium beats more favorably in the first quadrant. A decrease in the range of the effective stroke is seen, with the recovery stroke taking the cilium further towards the fourth quadrant (in a clockwise direction) than that of 4.8 (A). Perhaps this can be explained by the increase in the maximum value of Tug to 1.3748×10^{-7}. The effects are (proportionately) similar when k is increased to 0.40 (4.7 (C)) and to 0.45 (4.7 4.8 (D)). The maximum values of Tug for (C) and (D) are 2.0453×10^{-7} and 2.3645×10^{-7}, respectively. Clearly, as k is increased, the cilium bends more sharply and the recovery stroke takes the cilium further into the fourth quadrant. Since the maximum magnitude of shear angle indicates when the cilium is furthest from its starting position, it can be used to quantify how far (in a clockwise direction) the cilium goes into the fourth quadrant.

When $k = 0.10$ (4.7 (A)), the maximum magnitude of shear angle is 184.2283 degrees. When $k = 0.20$ (4.7 (B)), the maximum magnitude of shear angle is 192.0126 degrees. When $k = 0.40$ (4.7 (C)), the maximum magnitude of shear angle is 270.4095 degrees. When $k = 0.45$ (4.7 (D)), the maximum magnitude of shear angle is 302.0938 degrees.

4.1.1 Incorporating the Effects of Ca^{2+}

In order to model the effects of Ca^{2+}, a calcium term was added to the ODE for Tug ((4.3a) and (4.3b)):

$$\frac{dTug_{P_j}}{dt} = -k_1 \times f(v_j) - \left(k_2 \times \frac{[Ca^{2+}]}{[Ca^{2+}] + k_3}\right) \tag{4.8a}$$

$$\frac{dTug_{R_j}}{dt} = k_1 \times f(v_j) + \left(k_2 \times \frac{[Ca^{2+}]}{[Ca^{2+}] + k_3}\right) \tag{4.8b}$$

where j = segment. In equations (4.8a) and (4.8b), the Ca^{2+} term is derived from Michaelis-Menten kinetics. The constants k_2 and k_3 are modeling constants derived by an estimated best fit.

To implement the above equations, Euler's method was used with step size h=0.001 to obtain the following:

$$TugP_{j_n} = TugP_{j_{n-1}} - 0.001 \times k_1 \times f(v_{j_n}) - 0.001 \times k_2 \times TugP_{j_{n-1}} \times \frac{Ca^{2+}}{Ca^{2+} + k_3} \tag{4.9a}$$

$$TugR_{j_n} = TugR_{j_{n-1}} + 0.001 \times k_1 \times f(v_{j_n}) + 0.001 \times k_2 \times TugP_{j_{n-1}} \times \frac{Ca^{2+}}{Ca^{2+} + k_3} \tag{4.9b}$$

where n is the iteration/time step, with

$$0.00 \leq k_1 \leq 0.15, k_2 = 100.00, 0.00 < k_3 \leq 0.80$$

and v= sliding velocity ($\frac{ds}{dt}$), Ca^{2+}= calcium concentration.

The results from implementing the above equations into the Matlab simulation are given in the table below and in the figures following.

Table 4.2: The Effects of Ca^{2+} and Varying Dynein Force
*Simulations run with $f(v_j) = (v_j - v_0)^3$, $v_0 = -0.0300$, $k_1 = 0.08, k_2 = 100.00, k_3 = 0.50$

Value of Ca^{2+}	Duration of One Beat (iterations)	Min Sliding Velocity	Max Sliding Velocity	Min Tug	Max Tug
$Ca^{2+} = 0.10$	48	-0.0267	0.0344	0	1.4338×10^{-7}
$Ca^{2+} = 0.50$	42	-0.0279	0.0414	0	1.5508×10^{-7}
$Ca^{2+} = 0.80$	44	-0.0261	0.0481	0	1.6556×10^{-7}
$Ca^{2+} = 1.00$	46	-0.0261	0.0502	0	1.7170×10^{-7}

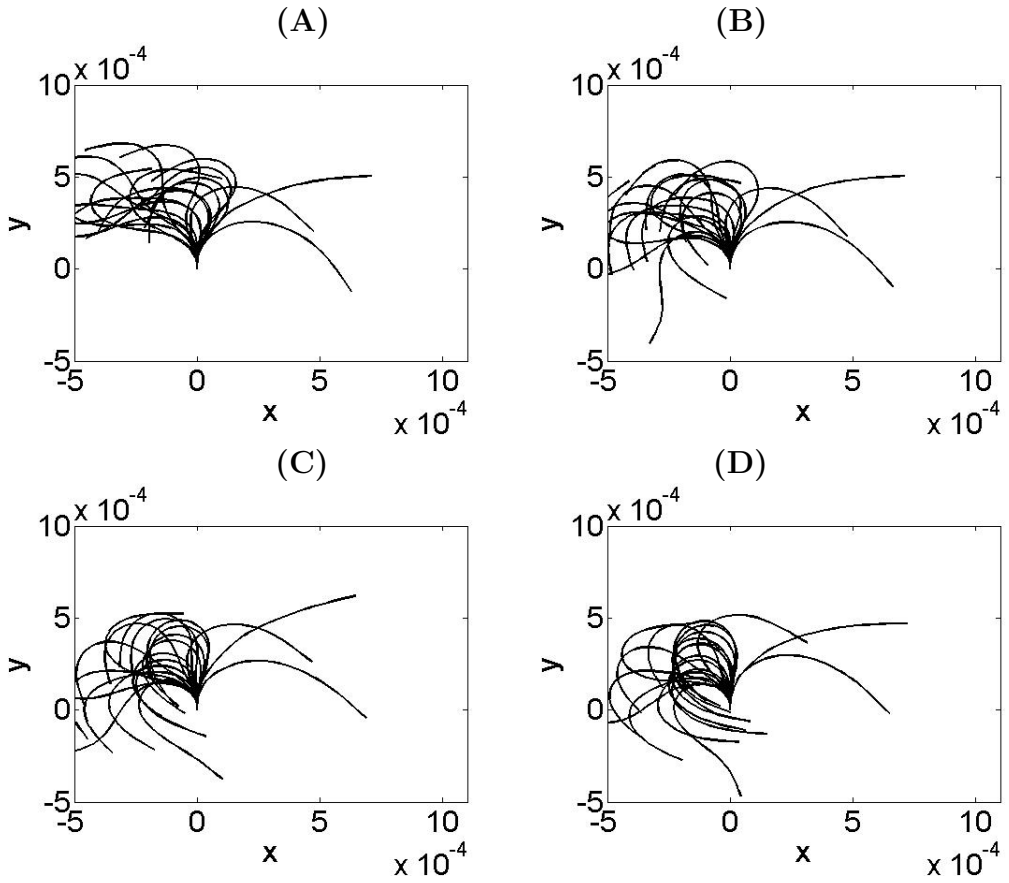

Figure 4.8: Varying Dynein Force + Ca^{2+} - Waveforms: (A) Ca^{2+} = 0.10, (B)Ca^{2+} = 0.50, (C) Ca^{2+} = 0.80, (D) Ca^{2+} = 1.00

Figure 4.8 shows the beatforms generated using various calcium concentrations. Upon the addition of a relatively small Ca^{2+} concentration of 0.10, the cilium beats noticeably more asymmetrically, as shown in 4.8 (A). Moreover, the direction of the effective and recovery strokes appear to "switch" during later time steps. When calcium concentration is increased to 0.50 (4.8 (B)), the cilium beats almost entirely in the second quadrant, and a complete switch in effective and recovery stroke direction is seen. The cilium also exhibits an overall increase in curvature at the more distal segments. This increase in curvature continues as calcium concentration is increased to 0.80 (4.8 (C)) and again to 1.00 (4.8 (D)). Though not shown in 4.8 (D), it is worth noting that when calcium concentration is set to 1.00 or above and the simulation is run for at least 200 time steps, the cilium eventually "arrests" by settling into a sharply curved position.

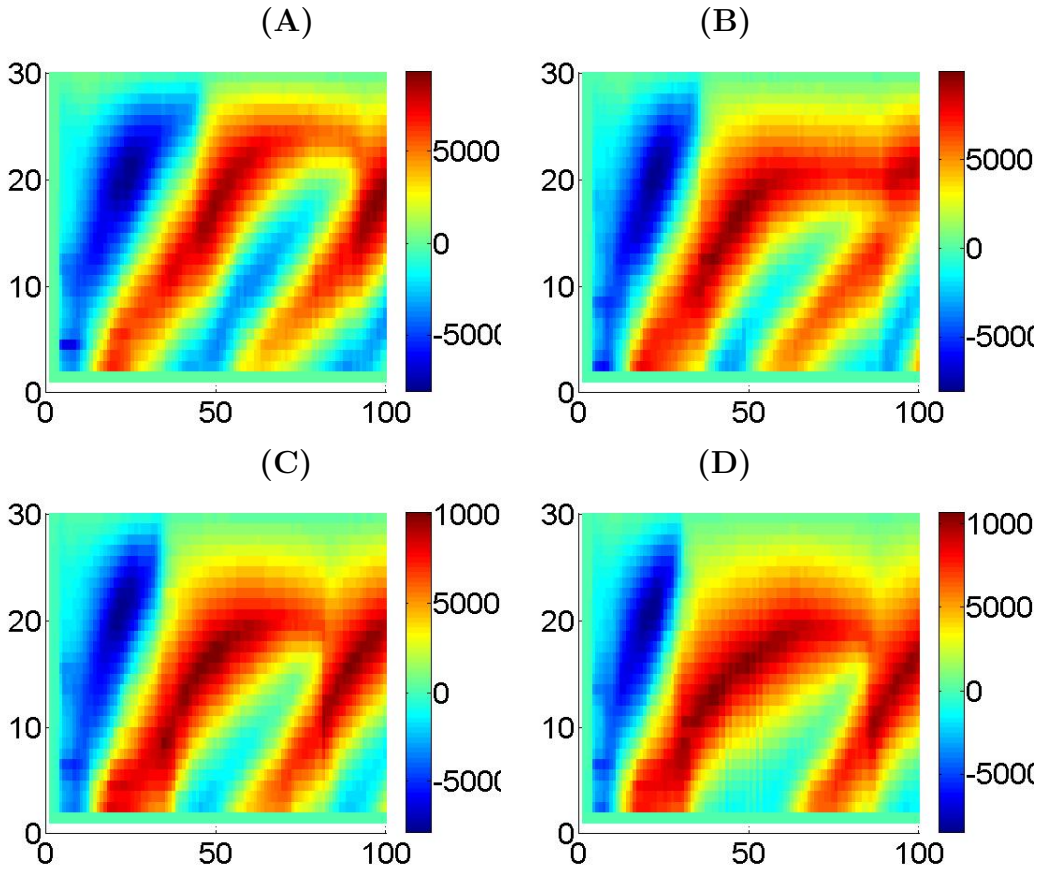

Figure 4.9: Varying Dynein Force + Ca^{2+} - Curvature: (A) Ca^{2+} = 0.10, (B)Ca^{2+} = 0.50, (C) Ca^{2+} = 0.80, (D) Ca^{2+} = 1.00

The curvature plots shown in figure 4.9 show the effects of various calcium concentrations on curvature. The x-axis represents time, going from 0 to 100 milliseconds, and the y-axis denotes the segment j. A notable pattern that emerged when a Ca^{2+} term was added was an overall increase in the magnitude of curvature as well as an overall reduction in the frequency of negative curvature. As the concentration of calcium is increased, as in 4.9 (A)-(D), the cilium bends more sharply and begins to bend in only direction. When a high concentration of calcium is used, such as that in 4.9 (D), it is evident that the cilium attains negative curvature only in the first thirty or so milliseconds. This is because the cilium "hooks" and curls to the left after about twenty milliseconds, where it remains for the rest of the simulation (see figure 4.8 (D)).

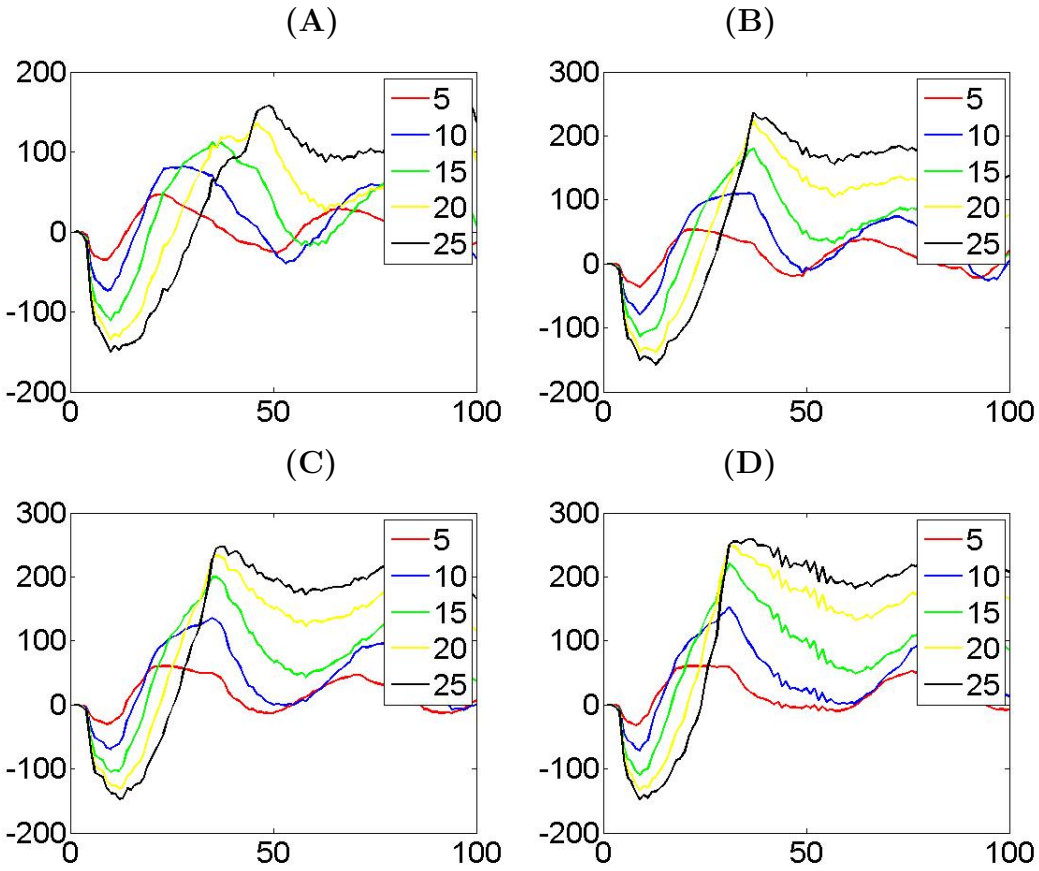

Figure 4.10: Varying Dynein Force + Ca^{2+} - Shear Angles: (A) $Ca^{2+} = 0.10$, (B)$Ca^{2+} = 0.50$, (C) $Ca^{2+} = 0.80$, (D) $Ca^{2+} = 1.00$

When analyzing the results of adding a calcium term to the ODE for Tug, shear angle was an important factor in interpreting the results. Figure 4.10 shows shear angle plotted along the y-axis versus time along the x-axis for four different calcium concentrations. Readily apparent from 4.10 (A), when calcium concentration is set to a low 0.10, there is an increase in the maximum shear angle attained. Since shear angle is a measure of the change in angle from the cilium's initial starting position (at ninety degrees) to it's current position, this increase in maximum shear angle indicates that the cilium is beating further into quadrants two and three than when no calcium is present. This effect continues as the calcium concentration is increased in 4.10 (B)-(D). Additionally, since the minimum shear angle attained by all four of (A)-(D) is generally consistent and non-changing, we may conclude that the addition of Ca^{2+} generates beatforms that mostly beat in the second and third quadrants. Though not shown in 4.10 (D), it is worthwhile to note that when run for at least 200 time steps, calcium concentrations of 1.00 or greater produced shear angle plots that "converged", or flattened-out towards the end of the simulation. This is consistent with the cilium settling into a fixed position, since the change in angle from it's initial position would be constant.

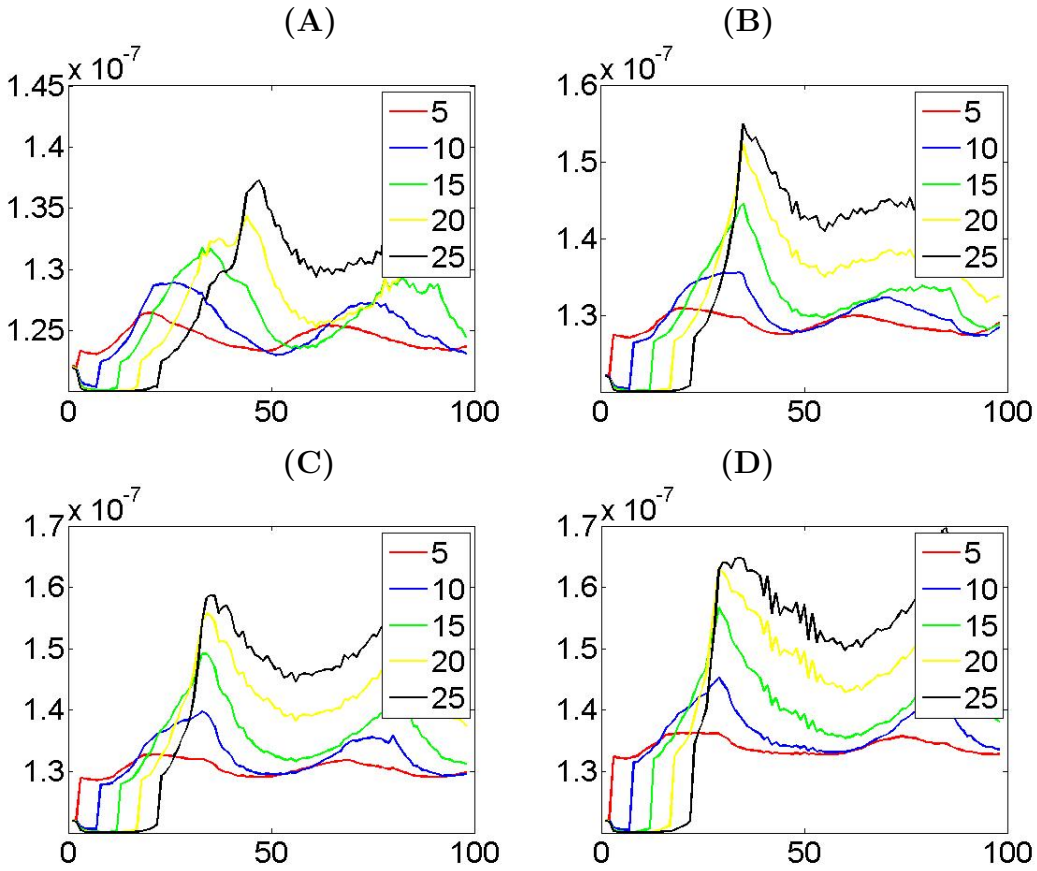

Figure 4.11: Varying Dynein Force + Ca^{2+} - Reverse Tug: (A) $Ca^{2+} = 0.10$, (B)$Ca^{2+} = 0.50$, (C) $Ca^{2+} = 0.80$, (D) $Ca^{2+} = 1.00$

Figures 4.11 and 4.12 show the effects of various calcium concentrations on the force exerted per dynein. 4.11 shows calculated values of Tug for reverse bend dyneins, and 4.12 shows calculated values of Tug for principal bend dyneins.The x-axis represents time (0-100 milliseconds), the y-axis represents the force per dynein (Tug), and the initial Tug value was set to 1.2×10^{-7} dyne for both principal and reverse Tug force. Tug values were taken at the fifth, tenth, fifteenth, twentieth, and twenty-fifth segments, and plotted in different colors. When the calcium concentration is set to just 0.10, as in 4.11 (A), the maximum Tug force is about 1.4×10^{-7}, a relatively small increase from the initial Tug force of 1.2×10^{-7}. As the calcium concentration is increased to 0.50 (4.11 (B)), 0.80 (4.11 (C)), and 1.00 (4.11 (D)), the maximum Tug force increases to about 1.5×10^{-7} (B), 1.6×10^{-7} (C), and 1.7×10^{-7} (D), respectively. Interestingly, this small change in Tug force results in dramatically different beatforms. This prompted further investigation into the stability of the Tug + Ca^{2+} ODE. However, there is a limit on Tug force due to the limiting $\frac{[Ca^{2+}]}{k_3+[Ca^{2+}]}$ term. This indicates that while the beatform may be sensitive to small changes in Tug force, the calculated values of Tug are still consistent with experimental data[22].

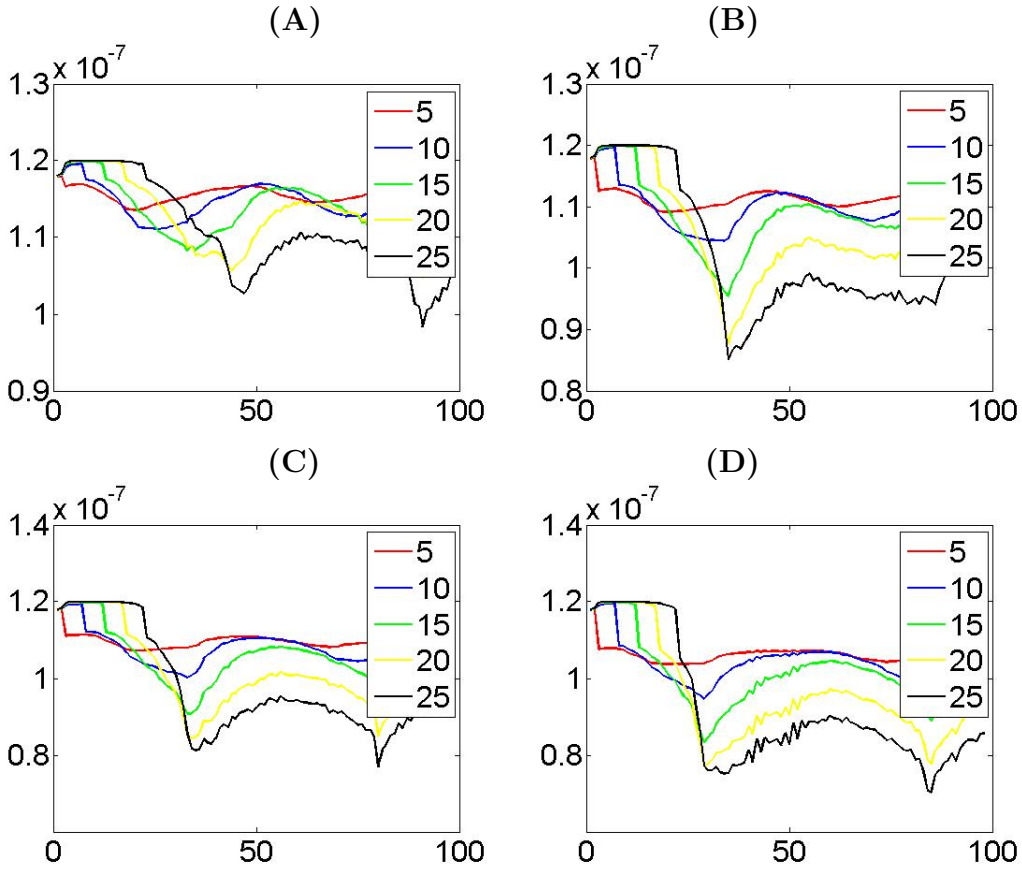

Figure 4.12: Varying Dynein Force + Ca^{2+} - Principal Tug: (A) $Ca^{2+} = 0.10$, (B)$Ca^{2+} = 0.50$, (C) $Ca^{2+} = 0.80$, (D) $Ca^{2+} = 1.00$

Chapter 5

Conclusions

The major findings of this study include three critical outcomes: the analysis of the original Geometric Clutch Hypothesis model, the proposal of an ordinary differential equation for dynein force, and the proposal of an ordinary differential equation for dynein force with the addition of calcium.

The analysis of the original GCH yielded valuble information as to the role of certain parameters. In studying the "unknown" parameters, or parameters that had no known experimental value and were "scaling" factors, results indicated that changing these parameter values could in turn change the beatform, beat frequency, curvature, and shear angle. Notable parameters that were analyzed include the transfer coefficient, the adhesion scaling factor, the t-force scaling factor, and the baseline probabilities of dynein attachment for the principle and reverse bends.

Next, an ODE for a varying time-dependent dynein force was proposed and implemented. The ODE uses the cilium's current sliding velocity to calculate the rate of change of Tug. Euler's method was used to implement the ODE, and since sliding velocity at each segment is known, it is treated as a constant. Four different velocity terms were tested, with $f(v_j) = (v_j - v_0)^3$ producing the most interesting and life-like beatforms. This function of velocity was chosen to ensure that Tug is constant when $v_j = v_0$ at some critical sliding velocity v_0. The value of v_0 was chosen to be the average minimum sliding velocity, since in the GCH a minimum in sliding velocity indicates a switch from effective to recovery stroke or vice versa. The results show an increase in curvature as well as an increase in the cilium's range of motion.

Finally, an ODE for a varying time-dependent dynein force with the addition of a calcium term was proposed and implemented. Euler's method was again used to solve for Tug at each time step, with the initial condition $TugP, R_j(0) = 1.2 \times 10^{-7}$. This equation also implemented $f(v_j) = (v_j - v_0)^3$ as the velocity term, and the results from using various concentrations of calcium were analyzed. The beatforms generated from four different Ca^{2+} concentrations ranging from 0.10 to 1.00 exhibited properties consistent with experimental data[8, 23, 1, 2]. Specifically, a direct relationship between calcium concentration and curvature was observed: as calcium concentration was increased, curvature also increased. Moreover, at higher conentrations of calcium (0.40-0.80), the directions of the effective and recovery strokes are "flipped" and mirrored across the y-axis. This behavior is consistent with experimental observations of increased asymmetry and a reversal of swimming direction in cilia and flagella at higher concentrations of calcium[2]. Finally, at Ca^{2+} concentrations greater than or equal to 1.00, the simulated cilium settles into a sharply curved position and eventually "arrests" after a sufficient time; this behavior is confirmed with observations from previous experiments[8].

The incorporation of a variable dynein force into the Geometric Clutch Hypothesis model of cil-

iary beating provided a deeper understanding of how dyneins work to regulate the bending of a cilium. Though dynein forces generated by the extended model are consistent with experimental measurements[22], further study of ciliary beating will be necessary to fully understand the mechanisms that regulate cilia and flagella. We hope this extended model provides insight regarding the role of dynein and calcium in ciliary beating and look forward to making further improvements in the future.

Appendix A

Equations

From Lindemann's Geometric Clutch Hypothesis

A.1 Geometric Clutch Hypothesis

A.1.1 Initial Variables

- n = number of segments (user-defined)
- Δs = segment length (cm)
- S_i = segments $i = 1, ..., n$
- D = diameter (cm)
- r = resting length of nexin (cm)
- h = stretched length of nexin (cm)
- dr = stretch of nexin (cm)
- I_0E = local passive stiffness (dyne cm^2)
- K_e = elastic constant of nexin per segment (dyne/cm)
- ϕ = angle formed by streched nexin with doublet axis (see diagram)
- Ψ = shear angle
- ds = interdoublet shear
- $\frac{d\theta}{ds}$ = curvature

A.1.2 Forces

- F_e = elastic force on nexin (passive)
- F_L = passive force component in the longitudinal direction
- F_T = passive force component in the transverse direction (transverse to axis of doublets)
- F_P = active force in principal bend
- F_R = active force in reverse bend
- F_{TOTAL} = total force (sum of active and passive)

A.1.3 Update shear angles and curvatures

- for i=2:n

$$\Psi(i) = \theta(i) - \theta(1)$$

$$\frac{d\theta}{ds}(i) = \frac{\theta(i) - \theta(i-1)}{\Delta s}$$

A.1.4 Calculating Passive Forces

1. Calculate ds

$$ds = \Psi \times D$$

2. Find h

$$h = \sqrt{r^2 + ds^2}$$

3. Calculate dr

$$dr = h - r$$

4. Find ϕ

$$\phi = \arctan(\frac{r}{ds})$$

5. Calculate F_e

$$F_e = K_e \times dr$$

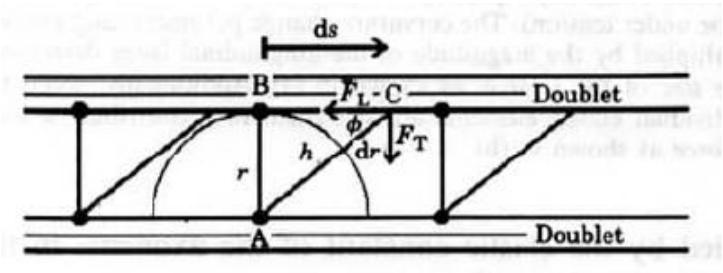

Figure A.1: Passive Forces

6. Calculate F_T and F_L

$$F_T = F_e \times sin\phi$$

$$F_L = F_e \times cos\phi \left(\frac{\Psi}{|\Psi|} \right)$$

A.1.5 Calculating Active Forces

1. Calculate t-forces

   - Initialize F_P and F_R at 0

$$t - force_P = F_T + \Delta s \times \left[\frac{d\theta}{ds} \times \sum_{i=1}^{n} (F_L + (1 - TC)F_P + (TC)F_R) \right]$$

$$t - force_R = F_T + \Delta s \times \left[\frac{d\theta}{ds} \times \sum_{i=1}^{n} (F_L + (1 - TC)F_R + (TC)F_P) \right]$$

   - TC = Transfer Coefficient

A.1.6 Torque and Total Forces

1. Calculate total force

$$F_{TOTAL} = 2 \times \sum F_L + \sum F_P + \sum F_R$$

2. Calculate torque

$$\frac{d\theta}{ds} \times I_0 E = F_{TOTAL} \times D$$

Appendix B

Matlab Code

```
%The Geometric Clutch Hypothesis with a Varying Dynein Force
clear all
close all
global L
global LM
param=zeros(1,25);
param=CiliumParameters(param);  %Load cilium parameter file
L=param(13);                    %Number of segments cilium is divided into
LM=L-1;
sx=zeros(1,L);                  %x locations of cilium
sy=zeros(1,L);                  %y locations of cilium
ang=(pi/2)*ones(1,L);           %Initialize angles
sang=zeros(1,LM);               %Initialize shear angles
cur=zeros(1,L);                 %Initialize curvatures

%Initializations
total=0;
Decay_C=2e10;
TotForce_R=.1;
TotForce_P=1;
Previous=0;
Push=0;
Adhesn_R=0;
DC=0;
tfa=zeros(4,LM);                %T-Forces: 1 & 2 are passive longitudinal
                                %and transverse components (respectively),
                                %3 and 4 are principal and reverse t-force
                                %components (respectively)
adh=zeros(2,LM);                %Adhesion force storage
forc=zeros(6,LM);               %Longitudinal forces on doublets (summed
                                %from distal end to basal body end)
dec=zeros(1,LM);                %Decay values
osx=zeros(1,L);                 %Old position data from previous iteration
```

```
osy=zeros(1,L);                 %-Same-
drag=zeros(1,LM);               %Drag-torque values
torq=zeros(1,LM);               %Total torque, passive and active
equ=zeros(1,LM);                %Equilibrium curvatures
adj=zeros(1,LM);                %Angle adjustments for feedback between
                                %iterations

%Loading parameters
param=CiliumParameters(param);
Diam=param(2);                  %Diameter
Tug=param(3);                   %Force per dynein
IE=param(4);                    %Passive stiffness of nexin
D=param(5);                     %Drag coefficient
Rn=param(6);                    %Resting length of nexin
Coupl=param(7);                 %Transfer coefficient
Switch_P=param(8);              %Baseline switching probability, principal
Switch_R=param(9);              %Baseline switching probability, reverse
Hister_P=param(10);             %Adhesion scaling factor, principl
Hister_R=param(11);             %Adhesion scaling factor, reverse
Gain=param(12);                 %T-Force scaling factor
L=param(13);
Z=param(14);                    %Segment length
Ke=param(15);                   %Elastic constant of nexin
Its=param(16);                  %Time step
N0=param(17);                   %No. of dyneins per segment

%More Initializations
State=1;
Base=1;
Route=1;
TriggerRoot_P=0;
TriggerRoot_R=0;

[sx sy cur sang]=startposSep(sx,sy,ang,cur,sang,Z);
osx=sx;
osy=sy;

N=100;                          %Number of iterations (100-1000)
Q=20;                           %Number of iterations per plot (1-20)

psi=zeros(N,LM);
angle=zeros(N,LM);
sangdeg=zeros(N,LM);
xpositions=zeros(N,L);
PRswitch=zeros(N,LM);
count=0;
```

```
dynslope=zeros(2,LM);
dyneinsP=zeros(N,LM);
dyneinsR=zeros(N,LM);
TugOldP=zeros(N,LM);
TugOldR=zeros(N,LM);
TugNewP=zeros(N,LM);
TugNewR=zeros(N,LM);
Vel=zeros(N,LM);

%Storage arrays for plotting
G=zeros(Q,L);
K=zeros(Q,L);
count1=1;
OlForce=1;
LR=1;

%Initializing movie setup
set(0,'defaultaxesfontsize',24);
scrsz = get(0,'ScreenSize');
fig1=figure(1);
winsize = get(fig1,'Position');
winsize(1:2) = [0 0];
set(fig1,'NextPlot','replacechildren')

%Begin main loop
for n=1:N
    if(n>1)
        figure(1)                          %Simulation of cilium
         plot(sx,sy,'-k','LineWidth',2.0)
         set(gcf,'Color','white')
         axis([-1.5e-3 1.1e-3 -0.5e-3 1e-3])
         hold on
         ndtime=Its*count;
         mytitle=['Testing GCH Cilia, n= ' num2str(n)];
         xlabel('x','FontWeight','bold');
         ylabel('y','FontWeight','bold');
   title(mytitle,'FontWeight','bold');
 hold off
 M(count1) = getframe;
         pause(.01)
         count=count+1;
         count1=count1+1;
    end

    %Variables that get zeroed-out at each iteration
    sang(1)=0;
```

```
cur(L)=0;
tfa=zeros(4,LM);
torq=zeros(1,LM);
equ=zeros(1,LM);
adj=zeros(1,LM);
phi=zeros(1,LM);

%Begin passive force calculations
  for j=1:LM                                    %j = segment #
    Hypot=sqrt((sang(j)*Diam)^2+(Rn)^2);
    ds(1,j)=(sang(j)*Diam);
    DR=Hypot-Rn;
    TF=Ke*DR;
    if(sang(j)==0)
        sang(j)=1e-6;
    end
    psi(n,j)=abs((atan(Rn/(sang(j)*Diam)))); %Angle formed by nexin in
                                             %relation to axis of
                                             %doublets
    tfa(1,j)=TF*cos(psi(n,j))*(sang(j)/abs(sang(j)));
    tfa(2,j)=TF*sin(psi(n,j));
    sangdeg(n,j)=((sang(j))/(pi/180));       %Convert shear angle from
                                             %radians to degrees
                                             %Shear angle: change in
                                             %angle from initial
                                             %segment angle

  end

%Summation loop for passive force
for j=1:LM
    SumF=0;
    for k=j:LM
        SumF=SumF+tfa(1,k);
    end
    forc(4,j)=SumF;
end

%Calculating active forces
for j=1:LM
    Long_Forc_P=forc(4,j)+forc(5,j)*(1-Coupl)+Coupl*forc(6,j);
    Long_Forc_R=forc(4,j)+forc(6,j)*(1-Coupl)+Coupl*forc(5,j);
    TVFP=tfa(2,j)+Z*cur(j+1)*Long_Forc_P;
    TVFR=tfa(2,j)+Z*cur(j+1)*Long_Forc_R;
    tfa(3,j)=TVFP;
    tfa(4,j)=TVFR;
```

```
TriggerRoot_P=Switch_P+((TVFP)*Gain);
TriggerRoot_R=Switch_R+((TVFR)*Gain);

%Calculating the varying dynein force
Vel(n,j)=(ds(1,j)/0.001);               %Sliding velocity
V0=-0.0300;                             %Avg. min. sliding velocity
k1=0.08;
%k2=100;
%k3=0.5;
%Ca=1.0;
if (1<=n<3)
    TugOldP(n,j)=Tug;
    TugOldR(n,j)=Tug;
elseif (n>=3)
    TugOldP(n,j)=TugP;
    TugOldR(n,j)=TugR;
end
%ODEs for principal and reverse dynein force
TugNewP(n,j)=TugOldP(n,j)-0.001*k1*((Vel(n,j)-V0)^3);
                        %-(0.001*k2*TugOldP(j)*(Ca/(Ca+k3)));
TugNewR(n,j)=TugOldR(n,j)+0.001*k1*((Vel(n,j)-V0)^3);
                        %+(0.001*k2*TugOldR(j)*(Ca/(Ca+k3)));

%Update Tug values
TugP=TugNewP(n,j);
TugR=TugNewR(n,j);

%Adhesion probability calculations
if(j==1)
    Trigger_R=TriggerRoot_R+adh(2,j)+0.5*adh(2,j+1);
elseif(j==LM)
    Trigger_R=TriggerRoot_R+adh(2,j)+0.5*adh(2,j-1);
else
    Trigger_R=TriggerRoot_R+adh(2,j)+0.5*adh(2,j-1)+0.5*adh(2,j+1);
end

if(Trigger_R<0)
    Trigger_R=0;
end

if(j==1)
    Trigger_P=TriggerRoot_P+adh(1,j)+0.5*adh(1,j+1);
elseif(j==LM)
    Trigger_P=TriggerRoot_P+adh(1,j)+0.5*adh(1,j-1);
else
    Trigger_P=TriggerRoot_P+adh(1,j)+0.5*adh(1,j-1)+0.5*adh(1,j+1);
```

```
end

if(Trigger_P<0)
    Trigger_P=0;
end

%Choice: are you in principal or reverse bend
Choice=abs(TotForce_R);
if(abs(TotForce_P)>=abs(TotForce_R))
    Choice=abs(TotForce_P);
end
counter=0;
Fac=2;
%Begin dynein bridge attachment loop
while(abs(Fac-1)>.1)
    counter=counter+1;
    if(counter>150)
        break;
    end
    OlForce=Choice;
    TotForce_P=0;
    TotForce_R=0;
    for bridge=1:N0
        R=rand(1,N0);
        BrVal=R(bridge);
        if(BrVal<Trigger_P)
            TotForce_P=TotForce_P+TugP;
        end
        P=rand(1,N0);
        BrVal=P(bridge);
        if(BrVal<Trigger_R)
            TotForce_R=TotForce_R-TugR;
        end
    end

%Update adhesion probabilities
Adhesn_P=abs(TotForce_P)*(1-TriggerRoot_P)*Hister_P;
Adhesn_R=abs (TotForce_R)*(1-TriggerRoot_R)*Hister_R;
adh(1,j)=Adhesn_P-Coupl*Adhesn_R;
adh(2,j)=Adhesn_R-Coupl*Adhesn_P;

if(j==1)
    Trigger_R=TriggerRoot_R+adh(2,j)+.5*adh(2,j+1);
elseif(j==LM)
    Trigger_R=TriggerRoot_R+adh(2,j)+0.5*adh(2,j-1);
else
```

```
        Trigger_R=TriggerRoot_R+adh(2,j)+0.5*adh(2,j-1)+.5*adh(2,j+1);
    end
        if (Trigger_R<0)
            Trigger_R = 0;
        end
    if(j==1)
            Trigger_P = TriggerRoot_P + adh(1,j)+.5*adh(1,j+1);
    elseif(j==LM)
            Trigger_P = TriggerRoot_P + adh(1,j)+.5*adh(1,j-1);
    else
            Trigger_P = TriggerRoot_P + adh(1,j)+.5*adh(1,j-1)+.5*adh(1,j+1);
    end
        if (Trigger_P<0)
            Trigger_P = 0;
        end

    forc(2,j) = TotForce_P;
    forc(3,j) = TotForce_R;

    %Calculate no. of attached dyneins
    if j>1
        dyneinsP(n,j)=(TotForce_P/TugP);
        dyneinsR(n,j)=abs(TotForce_R/TugR);
    end

    Choice = abs(TotForce_R);
    if (abs(TotForce_P)>=abs(TotForce_R))
        Choice=abs(TotForce_P);
    end
    if (OlForce == 0)
        OlForce=1e-6;
    end
    if (Choice == 0)
        Choice = OlForce;
    end
    Fac=Choice/OlForce;
    end
    counter;
end
%End of dynein bridge attachment loop

%Begin summation of forces and equilibrium curvatures
for i=1:LM                                  %Sum up forces from current
                                            %position to tip
    SUM_BP=0;
    SUM_BR=0;
```

```
                for j=i:LM
                    SUM_BP =SUM_BP+ forc(2,j);
                    SUM_BR =SUM_BR+ forc(3,j);
                end
        forc(5,i) = SUM_BP;
        forc(6,i) = SUM_BR;
    end
    %End active force calculations

%Begin torque and equilibrium curvature calculations
for j=1:LM
        forc(1,j) = 2*forc(4,j) + forc(5,j) + forc(6,j);
        torq(j)= forc(1,j)*Diam;
        equ(j)=-torq(j)/IE;
        OldDecay = dec(j);
        NewDecay = .6/(1+abs(drag(j)*Decay_C));
        if (n==1 && Route==1)
            NewDecay=.06;
        end
        if (n==2 && Route==1)
            NewDecay=.04;
        end
        if (n==3 && Route==1)
            NewDecay=.02;
        end
        Decay = (OldDecay + NewDecay)/2;
        dec(j)= Decay;
        adj(j)= (cur(j)-equ(j))*Decay;
end

%Begin drag loop
if (Base<1.0)
    AveBCorr = 0;
    TotCor = 0;
    RPTS = 0;
    drag(1) = 1e-6;
    Adjust = (Z/1e-4)^3;
    while ((abs(drag(1)))>=(1.4e-8*Adjust))
         Previous = drag(1);
         RPTS=RPTS+1;
         if (RPTS>100)
             exit(1);
         end
        j=1;
        DragTorque=0;
        DYDX=0;
```

```
        for k=(j+1):L
            Arm = sqrt((sx(j)-sx(k))^2+(sy(j)-sy(k))^2);
            VectX = sx(k)-osx(k);
            VectY = sy(k)-osy(k);
            if (VectX==0)
                VectX =1e-9;
            end
            DYDX = VectY/VectX;
            P_Angle =findangle(VectX, VectY, DYDX);
            MagN = sqrt(VectX^2+VectY^2);
            XLeg = sx(k)-sx(j);
            if (XLeg==0)
                XLeg=1e-9;
            end
            DYDX = (sy(k)-sy(j))/XLeg;
            L_Angle= findangle(XLeg, sy(k)-sy(j), DYDX);
            if (Arm==0)
                Arm = 1e-9;
            end
            Torque = Arm*DC*Z*((MagN*sin(P_Angle-L_Angle))/Its);
            DragTorque=DragTorque+Torque;
        end
    drag(1)=DragTorque;
    FeedBk = 6000/(D*Adjust);
    Push = drag(1)*FeedBk;
    AveBCorr = -Push;
    TotCor=TotCor+ AveBCorr;
    for j=1:LM
        ang(j)=ang(j)+AveBCorr;
        sx(j+1) = sx(j) + Z*cos(ang(j));
        sy(j+1) = sy(j) + Z*sin(ang(j));
    end
    if (RPTS>1 && (drag(1)*Previous)<0 )
        drag(1)=0.0;
    end
    end
    for j=1:LM
        ang(j)=ang(j)-TotCor*Base;
        sx(j+1)=sx(j)+Z*cos(ang(j));
        sy(j+1)=sy(j)+Z*sin(ang(j));
    end
end

if(Base<=1)
    for j=1:LM
        DragTorque=0;
```

```
        DYDX=0;
        for k=(j+1):L
        Arm = sqrt((sx(j)-sx(k))^2+(sy(j)-sy(k))^2);
        VectX = sx(k)-osx(k);
        VectY = sy(k)-osy(k);
        if (VectX==0)
            VectX =1e-9;
        end
        DYDX = VectY/VectX;
        P_Angle = findangle(VectX,VectY,DYDX);
        MagN=sqrt(VectX^2+VectY^2);
        XLeg = sx(k)-sx(j);
        if (XLeg==0)
            XLeg=1e-9;
        end
        DYDX = (sy(k)-sy(j))/XLeg;
        L_Angle= findangle(XLeg, sy(k)-sy(j), DYDX);
        if (Arm==0)
            Arm = 1e-9;
        end
        DC = .5*D+(.5*D*abs(sin(P_Angle-ang(k-1))));
        Torque=Arm*DC*Z*((MagN*sin(P_Angle-L_Angle))/Its);
        DragTorque=DragTorque+Torque;
        end
        drag(j)=DragTorque;
    end
    %End of drag loop

for i=2:LM                          %Major feedback point
        cur(i)=cur(i) - adj(i);
        ang(i)=ang(i-1) + cur(i)*Z;
        sang(i)=ang(i) - ang(1);
end

MatrixCur(:,n)=cur(:);              %Save curvatures in a matrix
for j=2:L                           %Recalculate positions
        osx(j)=sx(j);
        osy(j)=sy(j);
        sx(j)=sx(j-1)+Z*cos(ang(j-1));
        sy(j)=sy(j-1)+Z*sin(ang(j-1));
end
end
total=total+1;
end
%End of main loop
```

```
%Save simulation as a movie
movie(M);
save MtryDana.mat M
load MtryDana.mat
movie2avi(M, 'CiliaGCH.avi','fps',4)
```

Bibliography

[1] H Bannai, M Yoshimura, K Takahashi, and C Shingyoji. Calcium regulation of microtubule sliding in reactivated sea urchin sperm flagella. *Journal of Cell Science*, 113:831–839, 2000.

[2] CJ Brokaw. Calcium-induced asymmetrical beating of triton-demembranated sea urchin sperm flagella. *J Cell Bio*, 82:401–411, 1979.

[3] CJ Brokaw. Thinking about flagellar oscillation. *Cell Motility and the Cytoskeleton*, 66:425–436, 2009.

[4] CJ Brokaw and R Kamiya. Bending patterns of Chlaymydomonas flagella IV. mutants with defects in inner and outer dynein arms indicate differences in dynein arm funciton. *Cell Motil Cytoskel*, 8:68–75, 1987.

[5] Charles Daghlian. Mammalian lung sem. `http://remf.dartmouth.edu/images/mammalianLungSEM/image/lungtrachea1.jpg`, unknown. [Online; accessed 02/12/2013].

[6] CG DiPetrillo and EF Smith. Pcdp1 is a central apparatus protein that binds ca^{2+}-calmodulin and regulates ciliary motility. *Journal of Cell Biology*, 189:601–612, 2010.

[7] EA Gaffney, H Gadelha, DJ Smith, JR Blake, and JC Kirkman-Brown. Mammalian sperm motility: Observation and theory. *Annual Review of Fluid Mechanics*, 2011.

[8] BH Gibbons and IR Gibbons. Calcium-induced quiescence in reactivated sea urchin sperm. *J Cell Biol*, 84:13–27, 1980.

[9] CB Lindemann. A model of flagellar and ciliary functioning which uses the forces transverse to the axoneme as the regulator of dynein activation. *Cell Motil Cytoskel*, 29:141–154, 1994.

[10] CB Lindemann. Geometric clutch model version 3: The role of the inner and outer arm dyneins in the ciliary beat. *Cell Motility and the Cytoskeleton*, 52:242–254, 2002.

[11] CB Lindemann. Structural-functional relationships of the dynein, spokes, and central-pair projections predicted from an analysis of the forces acting within a flagellum. *Biophys J*, 84:4115–4126, 2003.

[12] CB Lindemann and AJ Hunt. Does axonemal dynein push, pull, or oscillate? *Cell Motil Cytoskeleton*, 56:237–244, 2003.

[13] CB Lindemann and KS Kanous. Geometric clutch hypothesis of axonemal function: key issues and testable predictions. *Cell Motil Cytoskel*, 31:1–8, 1995.

[14] CB Lindemann and KA Lesich. Flagellar and ciliary beating: the proven and the possible. *J Cell Science*, 123:519–528, 2010.

[15] H Lodish and A Berk. *Molecular Cell Biology*. W.H. Freeman, 1999. Figure 2.18 on page 819.

[16] T Mitchison and H Mitchison. How cilia beat. *Nature*, 463:308–309, 2010.

[17] National Institutes of Health. Human sperm cells. `http://img.bhs4.com/B8/8/B881EF68A4BD5B8FC07C41FFBF55A97F8C051B43_lis.jpg`, 2011. [Online; accessed 02/12/2013].

[18] KR Qin and C Xiang. Hysteresis modeling for calcium-mediated ciliary beat frequency in airway epithelial cells. *Mathematical Biosciences*, 229:101–108, 2011.

[19] JB Reece, L Urry, M Cain, S Wasserman, P Minorsky, and R Jackson. *Campbell Biology*. Harlow: Pearson Education, 2011.

[20] M Salathe. *Annu Rev Physiol*, 69:401–422, 2007.

[21] WS Sale. The axonemal axis and ca^{2+}-induced asymmetry of active microtubule sliding in sea urchin sperm tails. *Journal of Cell Biology*, 102:2042–2052, 1986.

[22] KA Schmitz, DL Holcomb-Wygle, DJ Oberski, and CB Lindemann. Measurement of the force produced by an intact bull sperm flagellum in isometric arrest and estimation of the dynein stall force. *Biophysical Journal*, 79:468–478, 2000.

[23] EF Smith. Regulation of flagellar dynein by calcium and a role for an axonemal calmodulin and calmodulin-dependent kinase. *Mol Biol Cell*, 13:3303–3313, 2002.